

Dark lens candidates from *Gaia* Data Release 3

K. Kruszyńska^{1,2,*}, Ł. Wyrzykowski¹, K. A. Rybicki³, K. Howil¹, M. Jabłońska^{1,4}, Z. Kaczmarek⁵, N. Ihanec¹,
M. Maskoliūnas⁶, M. Bronikowski⁷, and U. Pylypenko¹

¹ Astronomical Observatory, University of Warsaw, Al. Ujazdowskie 4, 00-478 Warszawa, Poland

² Las Cumbres Observatory, 6740 Cortona Drive, Suite 102, Goleta, CA 93117, USA

³ Department of Particle Physics and Astrophysics, Weizmann Institute of Science, Rehovot 76100, Israel

⁴ Research School of Astronomy and Astrophysics, Australian National University, Mount Stromlo Observatory, Cotter Road Weston Creek, ACT 2611, Australia

⁵ Zentrum für Astronomie der Universität Heidelberg, Astronomisches Rechen-Institut, Mönchhofstr. 12-14, 69120 Heidelberg, Germany

⁶ Institute of Theoretical Physics and Astronomy, Vilnius University, Saulėtekio al. 3, Vilnius, LT-10257, Lithuania

⁷ Center for Astrophysics and Cosmology, University of Nova Gorica, Vipavska 11c, SI-5270 Ajdovščina, Slovenia

Received xxxx; accepted xxxx

ABSTRACT

Gravitational microlensing is a phenomenon that allows us to observe dark remnants of stellar evolution even if they no longer emit electromagnetic radiation. In particular, it can be useful to observe solitary neutron stars or stellar-mass black holes, providing a unique window through which to understand stellar evolution. Obtaining direct mass measurements with this technique requires precise observations of both the change in brightness and the position of the microlensed star and the European Space Agency's *Gaia* satellite can provide both. We analysed events published in the *Gaia* Data Release 3 (*Gaia* DR3) microlensing catalogue using publicly available data from different surveys. Here we describe our selection of candidate dark lenses, where we suspect the lens is a white dwarf (WD), a neutron star (NS), a black hole (BH), or a mass-gap object, with a mass in a range between the heaviest NS and the least massive BH. We estimated the mass of the lenses using information obtained from the best-fitting microlensing models, the Galactic model and the expected distribution of the parameters. We found eight candidates for WDs or NS and two mass-gap objects.

Key words. Gravitational lensing: micro – Techniques: photometric – white dwarfs – Stars: neutron – Stars: black holes

1. Introduction

There are still many outstanding questions connected with the remnants of stellar evolution. The most common stellar remnant is a white dwarf, and more than 95 per cent will become one by the end of their life (Fontaine et al. 2001). Our understanding of white dwarfs was expanded in recent years by *Gaia* and its superb parallaxes. The largest catalogue consists of over 350'000 high-confidence WD candidates, expanding almost ten times the amount of known WDs before *Gaia* (Gentile Fusillo et al. 2021). The best catalogue of known pulsars is two orders of magnitude smaller than the one we have for WDs in our Galaxy (Manchester et al. 2005). Our most limited observational material is on BHs, in particular solitary ones. Most of the known BHs are linked to binary systems found either through X-ray emission due to accretion of their companions (e.g. Corral-Santana et al. 2016) or as gravitational wave sources due to their merger (e.g. Abbott et al. 2019). Additionally, gravitational wave mergers are detected most frequently in distant galaxies. Recently, Shenar et al. (2022), El-Badry et al. (2023b), and El-Badry et al. (2023a) have reported on BH candidates also detected as non-interacting binary systems. However, the only known direct mass measurement for a solitary stellar-mass BH was recently presented for OGLE-2011-BLG-0462/MOA-2011-BLG-191 (Sahu et al. 2022; Lam et al. 2022; Mróz et al. 2022; Lam & Lu 2023) using the gravitational microlensing phenomenon.

Gravitational microlensing is an effect of Einstein's General Relativity, which occurs when a massive object passes in front of a distant star within the Milky Way or its neighbourhood (Einstein 1936; Paczynski 1986). In contrast to strong gravitational lensing, here the separated, deformed images of the source are typically impossible to spatially resolve unless the world's largest telescopes are used, and only in case of very bright events (Dong et al. 2019; Cassan et al. 2022). Instead, what can be observed is a brightening of the source occurring during the event. Images of the source, though difficult to resolve, are unequally magnified and change position. This causes a distinctive shift in the centroid of light called astrometric microlensing (Dominik & Sahu 2000; Belokurov & Evans 2002). This effect can be measured with precise enough observatories like *Hubble* Space Telescope (HST) (Sahu et al. 2017), or *Gaia*¹.

Combining both effects allows the mass of the lens M_L to be measured following Gould (2000):

$$M_L = \frac{\theta_E}{\kappa\pi_E}, \quad (1)$$

where $\kappa = 4G/c^2 \text{au} \approx 8.144 \text{mas}/M_\odot$, θ_E is the angular Einstein Radius, which can be measured with astrometric microlensing, and π_E is the microlensing parallax obtained from modelling the time-series photometry. A combination of these two effects was used to detect a stellar-mass BH for the first time in Sahu et al.

* e-mail: kkruszyńska@lco.global

¹ https://www.cosmos.esa.int/web/gaia/iow_20210924

(2022) and Lam et al. (2022), who used astrometric observations from HST and photometric observations from the ground.

However, even without a measurement of the angular Einstein radius, we can still estimate the mass of the lens by employing the Galactic model and expected distributions of lens parameters. We can obtain a posterior distribution for the lens mass and distance using the microlensing parallax, proper motion measurements, estimated distance to the source, the Galactic model and assumed mass function of stellar remnants (e.g. Wyrzykowski et al. 2016; Mróz & Wyrzykowski 2021). This method was used for objects observed by the OGLE survey where no Einstein radius information was available, where events exhibited clear parallax signal (e.g. Wyrzykowski & Mandel 2020; Mróz et al. 2021). The same technique could also be applied for microlensing events seen by *Gaia* (Gaia Collaboration et al. 2016), using both archival data and transients detected as part of *Gaia* Science Alerts (GSA) system (Hodgkin et al. 2021). This paper presents a similar analysis of *Gaia* Data Release 3 (*Gaia* DR3) microlensing catalogue (Wyrzykowski et al. 2023).

This work is split into six sections. Section 2 presents the microlensing models compared in this work, the criteria of event pre-selection and the sources of data used for this analysis. Section 3 explains the criteria to select events for detailed analysis, while section 4 summarises those results. Section 5 shows how we estimated the masses and distances to the lenses. Section 6 discusses the obtained results and summarises this work.

2. Event pre-selection and data

2.1. Compared models

In this paper, we focused only on events that could exhibit the microlensing parallax effect, which occurs when the observer changes position during the event. There are three types of microlensing parallax: annual, terrestrial and space. The annual microlensing parallax is connected to the Earth's movement around the Sun. The observer on Earth changes their position during the entire year, which creates distinctive asymmetry and, in some cases, wobbles in the light curve (Gould 1992; Alcock et al. 1995; Maskoliūnas et al. 2023). The terrestrial parallax is connected to the different positions of the observatories on Earth. It is measurable only in the most extreme cases, such as catching a caustic crossing with telescopes on two sites distant from each other (Hardy & Walker 1995; Holz & Wald 1996; Gould et al. 2009). Finally, space parallax occurs when the event is observed from observatories located on Earth and in space. When the space observatory is located as far as one au from the Earth, it can cause a significant difference in the amplification and time of the peak of the lens (Refsdal 1966; Specht et al. 2023). It can be also measured if the space observatory is closer but during a caustic crossing (Wyrzykowski et al. 2020) or if the event is densely covered. This is the main mechanism behind the way that the Nancy Grace Roman Space Telescope is going to be used for mass measurements of the observed lenses (Penny et al. 2019).

Gaia DR3 microlensing events catalogue contains events which were most likely caused by a single object as an outcome of the used pipeline (Wyrzykowski et al. 2023). All of the events within this catalogue were detected in the Galactic plane, which is a dense field, especially within the Galactic bulge. This means that we had to include blending when some of the light is coming from the stars near the line of sight towards the source and lens.

In the case of microlensing, blending also factors in that the lens is luminous in the majority of cases.

We used the following models in our analysis with these parameters:

- point source - point lens (PSPL) model without blending, parameterised by t_0, u_0, t_E, I_0 ;
- PSPL with blending, parameterised by t_0, u_0, t_E, I_0, f_b ;
- PSPL model with parallax effect without blending, parameterised by $t_0, u_0, t_E, I_0, \pi_{EN}, \pi_{EE}$;
- PSPL model with a parallax effect with blending, parameterised by $t_0, u_0, t_E, \pi_{EN}, \pi_{EE}, I_0, f_b$;

where t_0 is the time of the peak of brightness, u_0 is the impact parameter at t_0 , and t_E is the Einstein timescale when the source is crossing the angular Einstein ring. Microlensing parallax is described by its northern and eastern components π_{EN} and π_{EE} . The baseline magnitude of the event is denoted by I_0 and the blending parameter is defined as $f_b = \frac{F_b}{F_s + F_b}$, where F_s is the source flux and F_b is the blend flux.

In this work, we used models without blending in the pre-selection stage, and for each event, we fitted models with and without parallax. We used models with blending when we fitted each event individually. At this stage, we also fitted models with and without parallax. Each event should have at least two best-fitting solutions: PSPL without blending, and PSPL with parallax and without blending.

2.2. Pre-selection of the candidate events

The *Gaia* Data Release 3, or alternatively table `vari_microlensing` of the *Gaia* DR3, contains 363 candidate events. Many of them do not exhibit second-order effects and are best described by the standard Paczyński model. We suspected that events with short Einstein timescales are less likely to be affected by the annual movement of the Earth around the Sun. Thus we selected events with `paczynski_0_te` timescale larger than 50 days. This was an arbitrary cut, based on the fact that *Gaia* produces on average one point per month per source. An event with an Einstein timescale of 50 days would last more than 100 days, allowing for at least 3 observations during the event. Additionally, previous studies of candidate parallax events show that in most cases parallax is not detectable for shorter events (see for example Rodriguez et al. (2022) and Zhai et al. (2023)). After applying this cut, we were left with 204 candidate events to analyse.

2.3. Data

The Wyrzykowski et al. (2023) catalogue was built using only *Gaia* G , G_{BP} and G_{RP} photometry, but for this work, we utilised data available from other surveys. In particular, we wanted to include information from microlensing surveys which have better cadence, especially in the Galactic bulge. We have cross-matched the *Gaia* sources with the OGLE survey (Udalski et al. 1992, 2015a). We have found 145 events in common with the public OGLE events. 130 events were published as a part of the OGLE-IV analysis of microlensing optical depth in the Galactic plane (Mróz et al. 2019, 2020). 78 events were published as also published as OGLE Early Warning System alerts (Udalski et al. 2015b), overlapping with the 130 events coming from the OGLE-IV papers. We downloaded all publicly available data. If the event was published in OGLE-EWS, Mróz et al. (2019) or Mróz et al. (2020), we used the data shared with the article. We

performed a similar search with MOA survey (Abe et al. 1997; Bond et al. 2001) using its alert stream and we found 20 events in common. We found 32 events in common with KMTNet survey public alerts (Lee et al. 2014; Kim et al. 2016). Six events were published by *Gaia* Science Alerts. These events were published with preliminary photometry and without errors. We simulated the errors using the following formula, (Wyrzykowski et al. 2023):

$$\sigma_{G,i} = \begin{cases} \sqrt{30} \times 10^{0.17 \times 13.5 - 5.1}, & \text{for } G_i < 13.5 \text{ mag,} \\ \sqrt{30} \times 10^{0.17 \times G_i - 5.1}, & \text{for } G_i \geq 13.5 \text{ mag,} \end{cases} \quad (2)$$

where G_i is the i -th point in the GSA light curve. Since the error bars and photometric data had different properties, they came from different pipelines, and GSA data was created using raw photometric data. *Gaia* DR3 light curves were created by the photometric pipeline that was used on all data used for this Data Release and produced the most accurate light curves we have. We decided to treat them as a different dataset. Seven events were found in the publicly available data of the ASAS-SN survey (Shappee et al. 2014). Two were published as alerts: ASASSN-16li and ASASSN-16oe (Strader et al. 2016; Munari et al. 2016), and one was published as an ATEL (Jayasinghe et al. 2017). The rest was found in the ASAS-SN Photometric Database (Jayasinghe et al. 2019). We did not include Zwicky Transient Facility (ZTF) (Bellm et al. 2019) while cross-matching events, because this survey started after May 2017, which was the end of *Gaia* DR3 timespan. We did however check for sources appearing in the 9th Data Release of ZTF if a given source brightened only once. The list of all 204 sources with their names in other surveys is available in Table A.1.

In the case of MOA and KMTNet, we have used the available photometry published in fluxes, instead of magnitudes. KMTNet is a network of three robotic telescopes, located in Australia, South Africa, and Chile. These sites have different weather conditions, and when we used KMTNet DIA photometry, we separated each light curve by the observatory. For *Gaia* photometry, we followed Wyrzykowski et al. (2023), and modified the available uncertainties to match the method used to find candidate events.

All data sources listed above were then used either at the preliminary or the detailed event modelling stages or both. We provide data used for this stage in a machine-readable online archive.

3. Selection of candidate events for further analysis

To find preliminary models, we used the `MuLensModel` package Poleski & Yee (2019) to generate microlensing models, and the `pyMultiNest` package (Feroz et al. 2009; Buchner et al. 2014) to find the best fitting solutions. To simplify the parameter space explored by the `pyMultiNest` package, we calculated models without blending. `pyMultiNest` provides a Python interface for a nested sampling algorithm which returns the best solutions for probability densities containing multiple modes and degeneracies. This made it a perfect tool for comparing models including microlensing parallax. For the parallax model, we included both the annual and space effects. *Gaia* is located in space, and there may be an offset between observatories.

We have recorded the four best solutions for models with and without parallax and compared their χ^2 values. These solutions are available in machine-readable format. Using preliminary models we selected events, that:

- had Einstein timescale of the best PSPL solution larger than 50 days, and
- the difference of χ^2 per degrees-of-freedom of the best PSPL model and the best parallax model should be larger than one ($\chi_{PSPL}^2/\text{dof} - \chi_{par}^2/\text{dof} > 1$).

This way we selected 34 events. We removed two events from this sample. For the first one (*Gaia*DR3-ULENS-024), we didn't have a full light curve, and the event did not finish before the end of the *Gaia* DR3 period. The second one (*Gaia*DR3-ULENS-178) turned out to be a binary event, when we inspected the MOA light curve. We decided to add three additional events, that had ASAS-SN data (*Gaia*DR3-ULENS-023, *Gaia*DR3-ULENS-032, and *Gaia*DR3-ULENS-118). In these cases, the automatic algorithm struggled to find a correct solution, and we concluded that was caused by the vastly different pixel size of the ASAS-SN, compared to *Gaia* and other surveys, and the exclusion of blending in fitted models.

4. Detailed analysis of selected events

We conducted a case-by-case analysis of the 35 events selected in the previous step. We used `MuLensModel` to generate the microlensing models and `emcee` (Foreman-Mackey et al. 2013) to explore the parameter space. In this step, we opted to use the KMTNet `pySIS` photometric data in magnitudes. For many events, we had to perform an outlier removal procedure. We have done this by fitting a preliminary PSPL model and removing all data points outside of the 3σ range of the residuals from the preliminary model. In some cases, we had to remove certain light curves, because they were too noisy. Table A.2 provides the name of the fitted event and a list of data sets with the amount of data points for each light curve. Table A.3 presents the median values of the posterior distributions (PDFs) obtained for best-fitting solutions. Here, we applied the following criteria to select the dark candidate events:

- the blending parameter in G band was smaller than 0.3,
- the π_E was not consistent with zero in the three-sigma range,
- the χ^2 of the parallax solution was smaller than the χ^2 of the non-parallax solution.

This way we obtained 16 events, where at least one solution passed those criteria. For these events, we then estimated the lens distance and mass. From the remaining events, nine were better described by a non-parallax model, five didn't pass the blending parameter criterion and for one, *Gaia*DR3-ULENS-057, we managed to only find a non-parallax solution.

5. Estimating lens parameters of the candidate dark events

We used the same approach as in Wyrzykowski et al. (2016), Mróz & Wyrzykowski (2021) and Kruszyńska et al. (2022) to estimate the mass and distance to the lens. We dubbed it the `DarkLensCode`² and we explained this method in greater detail in Howil et al. (2024, in prep.). The `DarkLensCode` was used to find the posterior distribution of lens distance and lens mass, using PDFs of the photometric model parameters, and the Galactic model. The final estimates are the median values of obtained mass and distance PDFs. Here we will focus on the presentation and of resulting mass and distance estimates. We present the results in Table 1.

² <https://github.com/BHTOM-Team/DarkLensCode>

If we found more than one solution passed the criteria outlined in Section 4, we combined the resulting posterior distribution into one, randomly selecting 50 000 points for each solution. We used three mass functions as lens mass priors: Kroupa (2001) function that describes stars:

$$f(M) \sim \begin{cases} M^{-0.3}, & M \leq 0.08 M_{\odot}, \\ M^{-1.3}, & 0.08 M_{\odot} < M \leq 0.5, \\ M^{-2.3}, & 0.5 M_{\odot} < M < 150 M_{\odot}, \end{cases} \quad (3)$$

Mróz et al. (2021) function that describes solitary dark remnants in our Galaxy:

$$f(M) \sim \begin{cases} M^{0.51}, & M \leq 1.0 M_{\odot}, \\ M^{-0.83}, & 1.0 M_{\odot} < M < 100 M_{\odot}, \end{cases} \quad (4)$$

and a $f(M) \sim M^{-1}$ corresponding to applying no prior on the lens function. The reported values of the lens mass and distance are median values of the posterior distribution, while their uncertainty is represented by the 16-th and 86-th quantiles.

We noticed that the mass function greatly affects the lens mass estimate. Using the Kroupa (2001) mass function results in lighter lenses at greater distances, and in turn more likely MS stars. In contrast, the Mróz et al. (2021) mass function produced more massive lenses at closer distances. This is because the Kroupa (2001) mass function is steeper and has a lower chance of producing massive lenses.

We also calculated the probability that the lens is dark and not an MS star. We compared the brightness of the blend from the microlensing model and compared it to the brightness of an MS star at an estimated distance from the lens, including (P_A) and excluding (P_0) extinction in that direction. The extinction A_G used for the calculation of the observed magnitude of an MS was taken, when possible, from *Gaia* DR3 (ag_phot value). Otherwise, we calculated A_G using the reddening maps of Schlafly & Finkbeiner (2011) and a relation of $E(B-V)$ with A_G from Wang & Chen (2019). We compared the A_G value to extinction in u' , g' , r' , and i' filters from Schlafly & Finkbeiner (2011) to confirm its validity. When we included extinction, it resulted in a lower probability for a dark lens. All input parameters are available in machine-readable form in an online archive attached to this paper.

6. Discussion and conclusions

We found four lenses for which the probability P_A for the dark lens scenario exceeded 80% when we looked only at the Kroupa (2001) mass function (*Gaia*DR3-ULENS-069, *Gaia*DR3-ULENS-088, *Gaia*DR3-ULENS-343, and *Gaia*DR3-ULENS-353) and included extinction. We can expand this list by six additional events when demanding that probability only the probability P_0 is larger than 80% (*Gaia*DR3-ULENS-155, *Gaia*DR3-ULENS-212, *Gaia*DR3-ULENS-259, *Gaia*DR3-ULENS-270, *Gaia*DR3-ULENS-363). The probability P_0 was calculated without including the extinction. All but one of these events have Galactic coordinates located near the Galactic Center. The estimated distance for all but one of these nine objects would suggest that they are located in the Galactic disc, rather than the Galactic bulge. This would mean, that the extinction should be smaller than the value used in this work. This in turn means, that it's less likely that the object would be an MS star, since the true brightness of an MS star $G_{MS,true}$ should lie between two marginal values calculated in this paper, namely $G_{MS,0} < G_{MS,true} < G_{MS,A}$. Additionally, these eight lenses

would belong to the Galactic disc population and five of them are located in the nearest 2.5 kpc radius. Only one lens, *Gaia*DR3-ULENS-212, seems to be located near the Galactic bulge and would belong to that population.

If we assumed that all of those nine events are dark lenses, and instead follow a Mróz et al. (2021) mass function, we would end up with the majority of events with masses in the range of white dwarfs and neutron stars. Two objects have slightly larger masses: *Gaia*DR3-ULENS-069 could be consistent with a mass-gap object, and *Gaia*DR3-ULENS-259 could be a mass-gap object or a light BH. *Gaia*DR3-ULENS-259 has also the largest uncertainty for its mass, the interval.

We present these estimates, comparing them to dark remnant mass estimates found through other methods in Figure 2.

In the case of events where *Gaia* reported a proper motion, we decided to calculate the transverse velocity. We present results for selected nine events in Figure 3. The more massive objects seem to have lower velocities than the less massive ones, but the error bars are large and it is hard to draw any conclusive statements. Moreover, here we are most likely getting an estimate of a velocity coming from a Galactic prior. More accurate estimates will be possible, once we obtain an astrometric time series for these events.

Here we also measure only the most likely mass of candidate events. We cannot however confirm their nature as WDs, NS or BHs until we perform additional observations in other ranges of the electromagnetic radiation, especially X-rays and UV. They could be some unusual objects, such as quark stars, or products of primordial black hole (PBH) mergers with other objects. Abramowicz et al. (2018) and Abramowicz et al. (2022) show a mechanism, that could produce a low-mass BH from a moon-mass PBH ($10^{25} \text{ g} > M_{PBH} > 10^{17} \text{ g}$) collision with a NS. Such low-mass BH would be in the mass range of a NS.

It is worth noting, that these are only candidates for dark lenses, and their mass measurement will be possible only when we will include astrometric time series. This data will be available only with *Gaia* DR4, no sooner than the end of 2025. This is an exciting prospect, as *Gaia* may allow us to observe previously unseen stellar populations. This becomes even more promising with the approaching start of the Vera C. Rubin Observatory and its Legacy Survey of Space and Time (Ivezić et al. 2019), as well as the launch of the Roman mission (Akeson et al. 2019; Spergel et al. 2015). Rubin will allow us to select long-duration microlensing events from the entire Galactic plane, while Roman can provide us with high-cadence astrometric and photometric observations in the Galactic bulge.

Acknowledgements. KK would like to thank Monika Sitek, Drs. Etienne Bachelet, Mariusz Gromadzki, Przemek Mróz, Radek Poleski, Milena Ratajczak, Rachel Street, Paweł Zieliński, Przemysław Mikołajczyk, as well as Profs. Michał Bejger, Wojciech Hellwing, Katarzyna Małek, and Łukasz Stawarz. This work was supported from the Polish NCN grants: Harmonia No. 2018/30/M/ST9/00311, Daina No. 2017/27/L/ST9/03221, and NCBiR grant within POWER program nr POWR.03.02.00-00-1001/16-00. LW acknowledges MNiSW grant DIR/WK/2018/12 and funding from the European Union's Horizon 2020 research and innovation program under grant agreement No. 101004719 (OPTICON-RadioNET Pilot, ORP). This work has made use of data from the European Space Agency (ESA) mission *Gaia* (<https://www.cosmos.esa.int/gaia>), processed by the *Gaia* Data Processing and Analysis Consortium (DPAC, <https://www.cosmos.esa.int/web/gaia/dpac/consortium>). Funding for the DPAC has been provided by national institutions, in particular, the institutions participating in the *Gaia* Multilateral Agreement. We acknowledge ESA *Gaia*, DPAC and the Photometric Science Alerts Team (<http://gsaweb.ast.cam.ac.uk/alerts>).

References

- Abbott, B. P., Abbott, R., Abbott, T. D., et al. 2019, *Phys. Rev. X*, 9, 031040
- Abbott, R., Abbott, T. D., Abraham, S., et al. 2021a, *Physical Review X*, 11, 021053
- Abbott, R., Abbott, T. D., Abraham, S., et al. 2021b, *SoftwareX*, 13, 100658
- Abe, F., Allen, W., Banks, T., et al. 1997, in *Variables Stars and the Astrophysical Returns of the Microlensing Surveys*, ed. R. Ferlet, J.-P. Maillard, & B. Raban, 75
- Abramowicz, M., Bejger, M., Udalski, A., & Wielgus, M. 2022, *ApJ*, 935, L28
- Abramowicz, M. A., Bejger, M., & Wielgus, M. 2018, *ApJ*, 868, 17
- Akeson, R., Armus, L., Bachelet, E., et al. 2019, *arXiv e-prints*, arXiv:1902.05569
- Alcock, C., Allsman, R. A., Alves, D., et al. 1995, *ApJ*, 454, L125
- Antoniadis, J. I. 2013, PhD thesis, Rheinische Friedrich Wilhelms University of Bonn, Germany
- Bellm, E. C., Kulkarni, S. R., Graham, M. J., et al. 2019, *PASP*, 131, 018002
- Belokurov, V. A. & Evans, N. W. 2002, *MNRAS*, 331, 649
- Bond, I. A., Abe, F., Dodd, R. J., et al. 2001, *MNRAS*, 327, 868
- Buchner, J., Georgakakis, A., Nandra, K., et al. 2014, *A&A*, 564, A125
- Cassan, A., Ranc, C., Absil, O., et al. 2022, *Nature Astronomy*, 6, 121
- Corral-Santana, J. M., Casares, J., Muñoz-Darias, T., et al. 2016, *A&A*, 587, A61
- Dominik, M. & Sahu, K. C. 2000, *ApJ*, 534, 213
- Dong, S., Mérand, A., Delplancke-Ströbele, F., et al. 2019, *ApJ*, 871, 70
- Einstein, A. 1936, *Science*, 84, 506
- El-Badry, K., Rix, H.-W., Cendes, Y., et al. 2023a, *MNRAS*, 521, 4323
- El-Badry, K., Rix, H.-W., Quataert, E., et al. 2023b, *MNRAS*, 518, 1057
- Feroz, F., Hobson, M. P., & Bridges, M. 2009, *MNRAS*, 398, 1601
- Fontaine, G., Brassard, P., & Bergeron, P. 2001, *PASP*, 113, 409
- Foreman-Mackey, D., Hogg, D. W., Lang, D., & Goodman, J. 2013, *PASP*, 125, 306
- Gaia Collaboration, Prusti, T., de Bruijne, J. H. J., et al. 2016, *A&A*, 595, A1
- Gentile Fusillo, N. P., Tremblay, P. E., Cukanovaite, E., et al. 2021, *MNRAS*, 508, 3877
- Gould, A. 1992, *ApJ*, 392, 442
- Gould, A. 2000, *ApJ*, 542, 785
- Gould, A., Udalski, A., Monard, B., et al. 2009, *ApJ*, 698, L147
- Hardy, S. J. & Walker, M. A. 1995, *MNRAS*, 276, L79
- Hobbs, G., Lorimer, D. R., Lyne, A. G., & Kramer, M. 2005, *MNRAS*, 360, 974
- Hodgkin, S. T., Harrison, D. L., Breedt, E., et al. 2021, *A&A*, 652, A76
- Holz, D. E. & Wald, R. M. 1996, *ApJ*, 471, 64
- Ivezić, Ž., Kahn, S. M., Tyson, J. A., et al. 2019, *ApJ*, 873, 111
- Jabłońska, M., Wyrzykowski, Ł., Rybicki, K. A., et al. 2022, *arXiv e-prints*, arXiv:2206.11342
- Jayasinghe, T., Kochanek, C. S., Stanek, K. Z., et al. 2017, *The Astronomer's Telegram*, 10677, 1
- Jayasinghe, T., Stanek, K. Z., Kochanek, C. S., et al. 2019, *MNRAS*, 485, 961
- Kaczmarek, Z., McGill, P., Evans, N. W., et al. 2022, *MNRAS*, 514, 4845
- Kim, S.-L., Lee, C.-U., Park, B.-G., et al. 2016, *Journal of Korean Astronomical Society*, 49, 37
- Kroupa, P. 2001, *MNRAS*, 322, 231
- Kruszyńska, K., Wyrzykowski, Ł., Rybicki, K. A., et al. 2022, *A&A*, 662, A59
- Lam, C. Y. & Lu, J. R. 2023, *ApJ*, 955, 116
- Lam, C. Y., Lu, J. R., Udalski, A., et al. 2022, *ApJ*, 933, L23
- Lattimer, J. M. 2012, *Annual Review of Nuclear and Particle Science*, 62, 485
- Lee, C.-U., Kim, S.-L., Cha, S.-M., et al. 2014, in *Society of Photo-Optical Instrumentation Engineers (SPIE) Conference Series*, Vol. 9145, *Ground-based and Airborne Telescopes V*, ed. L. M. Stepp, R. Gilmozzi, & H. J. Hall, 91453T
- Manchester, R. N., Hobbs, G. B., Teoh, A., & Hobbs, M. 2005, *AJ*, 129, 1993
- Maskoliūnas, M., Wyrzykowski, Ł., Howil, K., et al. 2023, *arXiv e-prints*, arXiv:2309.03324
- Miller-Jones, J. C. A., Bahramian, A., Orosz, J. A., et al. 2021, *Science*, 371, 1046
- Mróz, P., Udalski, A., & Gould, A. 2022, *ApJ*, 937, L24
- Mróz, P., Udalski, A., Skowron, J., et al. 2019, *ApJS*, 244, 29
- Mróz, P., Udalski, A., Szymański, M. K., et al. 2020, *ApJS*, 249, 16
- Mróz, P., Udalski, A., Wyrzykowski, Ł., et al. 2021, *arXiv e-prints*, arXiv:2107.13697
- Mróz, P. & Wyrzykowski, Ł. 2021, *Acta Astron.*, 71, 89
- Munari, U., Hamsch, F. J., & Frigo, A. 2016, *The Astronomer's Telegram*, 9879, 1
- Orosz, J. A., McClintock, J. E., Narayan, R., et al. 2007, *Nature*, 449, 872
- Orosz, J. A., Steeghs, D., McClintock, J. E., et al. 2009, *ApJ*, 697, 573
- Orosz, J. A., Steiner, J. F., McClintock, J. E., et al. 2014, *ApJ*, 794, 154
- Paczynski, B. 1986, *ApJ*, 304, 1
- Penny, M. T., Gaudi, B. S., Kerins, E., et al. 2019, *ApJS*, 241, 3
- Poleski, R. & Yee, J. C. 2019, *Astronomy and Computing*, 26, 35
- Refsdal, S. 1966, *MNRAS*, 134, 315
- Rodríguez, A. C., Mróz, P., Kulkarni, S. R., et al. 2022, *ApJ*, 927, 150
- Sahu, K. C., Anderson, J., Casertano, S., et al. 2017, *Science*, 356, 1046
- Sahu, K. C., Anderson, J., Casertano, S., et al. 2022, *ApJ*, 933, 83
- Schlafly, E. F. & Finkbeiner, D. P. 2011, *ApJ*, 737, 103
- Shappee, B. J., Prieto, J. L., Grupe, D., et al. 2014, *ApJ*, 788, 48
- Shenar, T., Sana, H., Mahy, L., et al. 2022, *Nature Astronomy*, 6, 1085
- Specht, D., Poleski, R., Penny, M. T., et al. 2023, *MNRAS*, 520, 6350
- Spergel, D., Gehrels, N., Baltay, C., et al. 2015, *arXiv e-prints*, arXiv:1503.03757
- Strader, J., Chomiuk, L., Stanek, K. Z., et al. 2016, *The Astronomer's Telegram*, 9860, 1
- The LIGO Scientific Collaboration, the Virgo Collaboration, Abbott, R., et al. 2021a, *arXiv e-prints*, arXiv:2108.01045
- The LIGO Scientific Collaboration, the Virgo Collaboration, the KAGRA Collaboration, et al. 2021b, *arXiv e-prints*, arXiv:2111.03606
- Udalski, A., Szymanski, M., Kaluzny, J., Kubiak, M., & Mateo, M. 1992, *Acta Astron.*, 42, 253
- Udalski, A., Szymański, M. K., & Szymański, G. 2015a, *Acta Astron.*, 65, 1
- Udalski, A., Szymański, M. K., & Szymański, G. 2015b, *Acta Astron.*, 65, 1
- Val-Baker, A. K. F., Norton, A. J., & Negueruela, I. 2007, in *American Institute of Physics Conference Series*, Vol. 924, *The Multicolored Landscape of Compact Objects and Their Explosive Origins*, ed. T. di Salvo, G. L. Israel, L. Piersant, L. Burderi, G. Matt, A. Tornambe, & M. T. Menna, 530–533
- Wang, S. & Chen, X. 2019, *ApJ*, 877, 116
- Wyrzykowski, Ł., Kostrzewa-Rutkowska, Z., Skowron, J., et al. 2016, *MNRAS*, 458, 3012
- Wyrzykowski, Ł., Kruszyńska, K., Rybicki, K. A., et al. 2023, *A&A*, 674, A23
- Wyrzykowski, Ł. & Mandel, I. 2020, *A&A*, 636, A20
- Wyrzykowski, Ł., Mróz, P., Rybicki, K. A., et al. 2020, *A&A*, 633, A98
- Zhai, R., Rodríguez, A. C., Lam, C. Y., et al. 2023, *arXiv e-prints*, arXiv:2311.18627

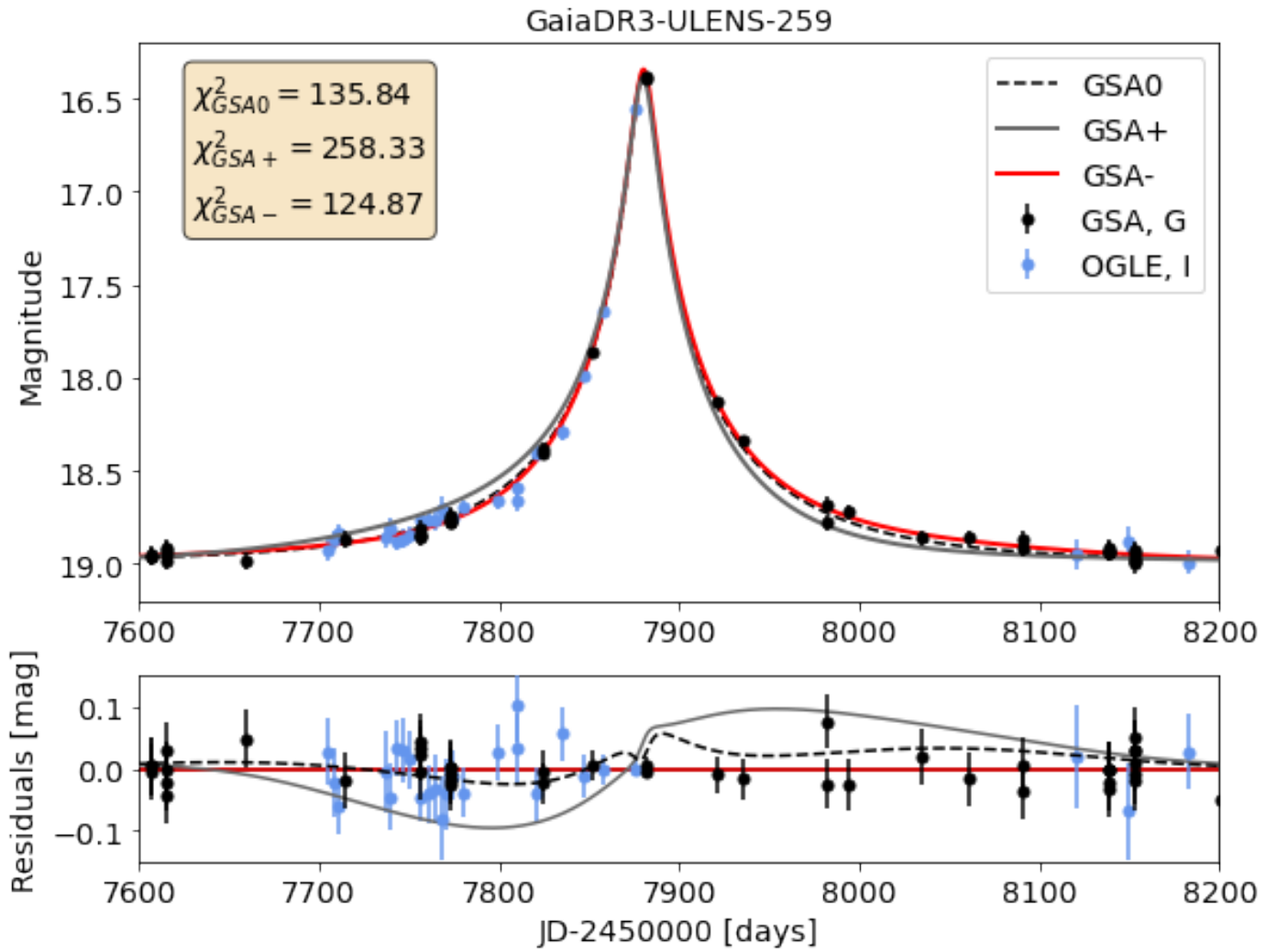


Fig. 1. Top panel: light curve of the event known as GaiaDR3-ULENS-259, Gaia17aqu, and BLG519.09.44226 (Mróz et al. 2020). *Gaia* Science Alerts data is shown in black, and OGLE in light-blue. Three best solutions are marked: PSPL without parallax GSA0 with a black dashed line, and two PSPL with parallax, GSA+ and GSA- with red and gray continuous lines respectively. The bracket in top left shows the χ^2 of different solutions. Bottom panel: Residuals of the GSA+ model. Black dashed line marks the GSA0 and GSA+ models difference, while the grey continuous line marks the GSA- and GSA+ models difference.

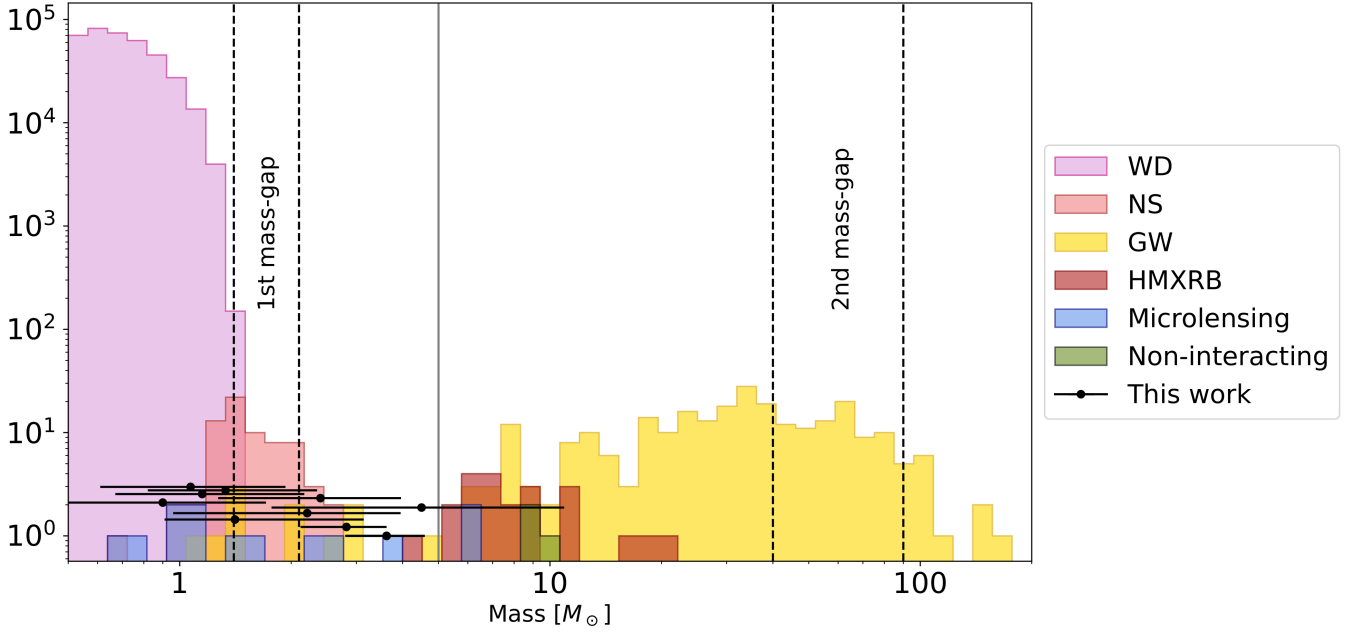


Fig. 2. Distribution of known masses of WDs, NS and BHs. Light pink marks WDs known from *Gaia* Gentile Fusillo et al. (2021). In light red we marked NS with known masses coming from John Antoniadis’s catalogue (Lattimer 2012; Antoniadis 2013). Objects found by gravitational wave detectors were marked in yellow (Abbott et al. 2019; Abbott et al. 2021a; The LIGO Scientific Collaboration et al. 2021a,b; Abbott et al. 2021b). In red we marked high mass x-ray binaries (Orosz et al. 2007; Val-Baker et al. 2007; Orosz et al. 2009, 2014; Corral-Santana et al. 2016; Miller-Jones et al. 2021). In light blue, we marked candidates for dark remnants found by microlensing (Mróz & Wyrzykowski 2021; Kaczmarek et al. 2022; Kruszyńska et al. 2022; Jabłońska et al. 2022), including Lam & Lu (2023). In olive, we marked non-interacting dark remnants (Shenar et al. 2022; El-Badry et al. 2023b,a). Black dots mark masses of objects known from this work.

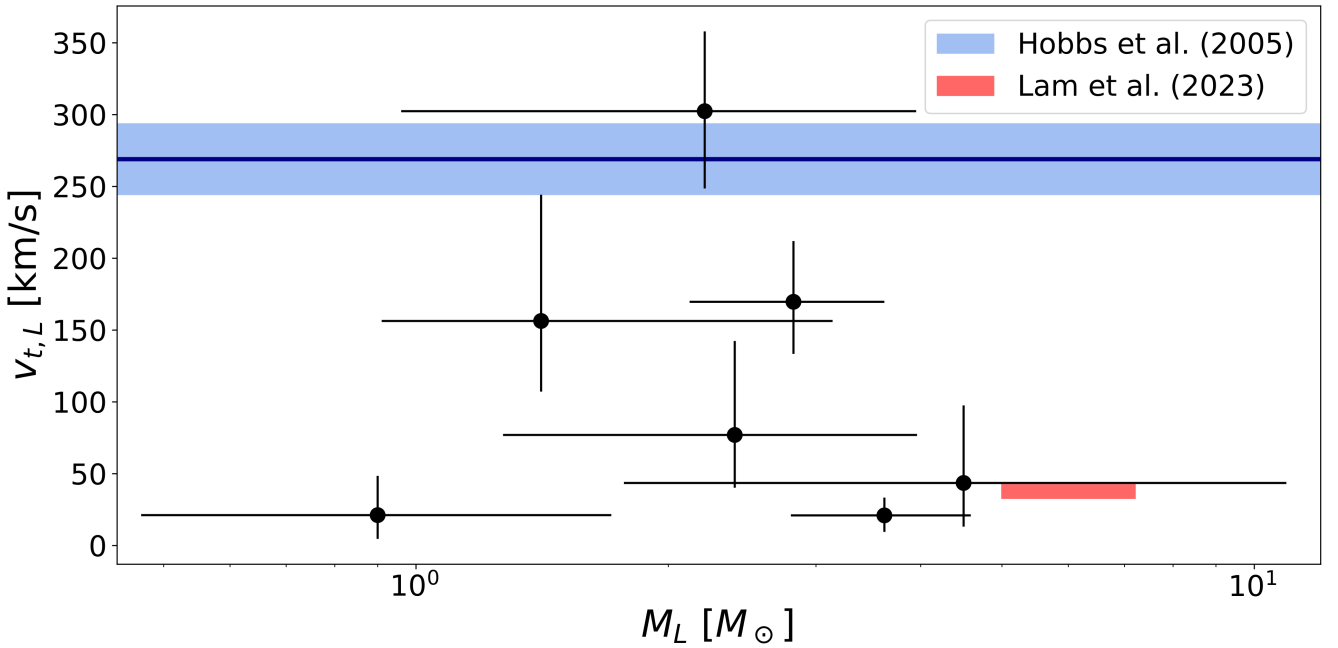


Fig. 3. Transverse velocities $v_{t,L}$ estimated for nine candidate events using DarkLensCode and *Gaia* proper motion measurements. M_L is the mass of the lens. Black dots represent estimates of the masses and velocities of the nine candidates with error bars as lines. The blue line represents the median transverse velocity of NS from Hobbs et al. (2005), with a light blue rectangle representing their dispersion. The red rectangle represents the mass and transverse velocity of the BH from Lam & Lu (2023).

Table 1. Table of the lens mass and distance estimates of the 16 candidate dark lens microlensing events. The columns are event name, extinction in G filter A_G , mass function MF used as a prior for lens mass, distance to the lens D_L in kpc, the mass of the lens M_L in solar masses, the brightness of an MS star with M_L mass at a distance D_L without including extinction, the mass of the lens M_L in Solar masses, the brightness of an MS star with M_L mass at a distance D_L including extinction A_G , the brightness of the blend G_{blend} obtained from the microlensing model, probability for a dark lens P_A with extinction included, and the probability for a dark lens P_0 without including extinction. In the MF column, K2001 refers to Kroupa (2001), and M2021 to Mróz et al. (2021).

GaiaDR3- ULENS	A_G [mag]	MF	D_L [kpc]	M_L [M_\odot]	$G_{\text{MS},0}$ [mag]	$G_{\text{MS},A}$ [mag]	G_{blend} [mag]	P_A [%]	P_0 [%]
025	4.29	K2001	$0.73^{+0.59}_{-0.35}$	$0.47^{+0.39}_{-0.27}$	$18.29^{+3.77}_{-4.47}$	$22.58^{+3.77}_{-4.47}$	$19.31^{+1.29}_{-0.84}$	24.7	61.0
		M2021	$0.43^{+0.45}_{-0.19}$	$1.00^{+0.68}_{-0.49}$	$13.05^{+4.84}_{-3.57}$	$17.34^{+4.84}_{-3.57}$		68.7	90.4
		$\sim M^{-1}$	$0.68^{+0.60}_{-0.36}$	$0.54^{+0.69}_{-0.31}$	$17.50^{+4.06}_{-6.09}$	$21.78^{+4.06}_{-6.09}$		36.3	66.3
069	2.11	K2001	$5.94^{+0.78}_{-0.77}$	$3.24^{+0.95}_{-0.88}$	$13.95^{+0.96}_{-0.82}$	$18.24^{+0.96}_{-0.82}$	$22.53^{+1.49}_{-0.99}$	97.5	99.5
		M2021	$5.73^{+0.70}_{-0.74}$	$3.62^{+0.97}_{-0.82}$	$13.60^{+0.83}_{-0.77}$	$17.89^{+0.83}_{-0.77}$		99.6	100.0
		$\sim M^{-1}$	$5.77^{+0.71}_{-0.73}$	$3.59^{+0.95}_{-0.83}$	$13.63^{+0.86}_{-0.76}$	$17.92^{+0.86}_{-0.76}$		99.5	99.9
088	1.76	K2001	$3.95^{+2.01}_{-0.67}$	$2.45^{+0.77}_{-1.21}$	$13.75^{+3.71}_{-0.98}$	$15.51^{+3.71}_{-0.98}$	$20.14^{+0.31}_{-0.25}$	88.7	94.6
		M2021	$3.68^{+0.72}_{-0.61}$	$2.82^{+0.80}_{-0.70}$	$13.29^{+0.95}_{-0.94}$	$15.05^{+0.95}_{-0.94}$		98.2	99.5
		$\sim M^{-1}$	$3.71^{+0.74}_{-0.60}$	$2.79^{+0.77}_{-0.70}$	$13.32^{+0.99}_{-0.91}$	$15.08^{+0.99}_{-0.91}$		97.3	99.0
089	7.19	K2001	$1.21^{+0.56}_{-0.43}$	$0.43^{+0.29}_{-0.17}$	$19.76^{+2.36}_{-3.67}$	$22.82^{+2.36}_{-3.67}$	$19.41^{+0.32}_{-0.24}$	17.6	46.8
		M2021	$0.78^{+0.51}_{-0.27}$	$0.84^{+0.90}_{-0.44}$	$14.92^{+5.19}_{-4.20}$	$17.98^{+5.19}_{-4.20}$		59.2	79.6
		$\sim M^{-1}$	$1.15^{+0.55}_{-0.50}$	$0.45^{+0.61}_{-0.17}$	$19.49^{+2.43}_{-6.19}$	$22.55^{+2.43}_{-6.19}$		27.4	49.6
097	3.99	K2001	$2.56^{+0.82}_{-0.78}$	$0.56^{+0.36}_{-0.25}$	$20.17^{+2.53}_{-3.18}$	$24.16^{+2.53}_{-3.18}$	$18.24^{+1.04}_{-0.44}$	3.3	30.6
		M2021	$2.70^{+1.20}_{-0.98}$	$1.04^{+1.23}_{-0.47}$	$16.39^{+3.77}_{-2.83}$	$20.38^{+3.77}_{-2.83}$		21.5	70.8
		$\sim M^{-1}$	$2.64^{+0.99}_{-0.86}$	$0.66^{+0.80}_{-0.32}$	$19.21^{+3.21}_{-4.44}$	$23.20^{+3.21}_{-4.44}$		11.4	45.2
118	1.06	K2001	$0.41^{+0.39}_{-0.20}$	$0.27^{+0.31}_{-0.15}$	$18.95^{+3.94}_{-4.30}$	$20.00^{+3.94}_{-4.30}$	$19.62^{+1.29}_{-0.71}$	49.5	59.3
		M2021	$0.23^{+0.18}_{-0.07}$	$0.57^{+0.32}_{-0.28}$	$14.87^{+3.76}_{-3.28}$	$15.93^{+3.76}_{-3.28}$		84.0	89.7
		$\sim M^{-1}$	$0.43^{+0.51}_{-0.22}$	$0.26^{+0.32}_{-0.16}$	$19.10^{+4.94}_{-4.40}$	$20.16^{+4.94}_{-4.40}$		47.3	56.6
142	0.40	K2001	$5.95^{+0.73}_{-0.85}$	$0.88^{+0.42}_{-0.29}$	$19.28^{+2.68}_{-2.46}$	$19.68^{+2.68}_{-2.46}$	$20.83^{+1.49}_{-1.00}$	69.7	75.0
		M2021	$5.57^{+0.70}_{-3.94}$	$1.22^{+0.62}_{-0.36}$	$17.29^{+2.23}_{-3.21}$	$17.69^{+2.23}_{-3.21}$		91.4	93.5
		$\sim M^{-1}$	$5.70^{+0.78}_{-3.54}$	$1.09^{+0.59}_{-0.39}$	$17.93^{+2.86}_{-2.66}$	$18.33^{+2.86}_{-2.66}$		82.7	85.7
155	1.6	K2001	$2.99^{+0.82}_{-0.68}$	$0.92^{+0.54}_{-0.30}$	$17.45^{+2.55}_{-2.19}$	$19.05^{+2.55}_{-2.19}$	$19.97^{+0.17}_{-0.12}$	64.6	84.7
		M2021	$3.34^{+1.74}_{-0.94}$	$1.41^{+1.73}_{-0.50}$	$15.46^{+2.16}_{-2.09}$	$17.06^{+2.16}_{-2.09}$		90.7	97.3
		$\sim M^{-1}$	$3.19^{+1.39}_{-0.83}$	$1.24^{+1.14}_{-0.47}$	$15.94^{+2.63}_{-2.19}$	$17.54^{+2.63}_{-2.19}$		82.4	93.1
212	2.99	K2001	$8.15^{+0.15}_{-0.90}$	$0.89^{+0.95}_{-0.31}$	$19.95^{+2.64}_{-3.58}$	$22.94^{+2.64}_{-3.58}$	25.00	77.6	98.8
		M2021	$7.31^{+0.92}_{-0.98}$	$2.21^{+1.74}_{-1.25}$	$15.29^{+4.25}_{-1.59}$	$18.27^{+4.25}_{-1.59}$		96.8	99.9
		$\sim M^{-1}$	$7.71^{+0.55}_{-1.23}$	$1.61^{+1.95}_{-0.83}$	$16.91^{+3.86}_{-2.92}$	$19.89^{+3.86}_{-2.92}$		91.4	99.4
259	1.93	K2001	$2.24^{+1.37}_{-0.99}$	$1.21^{+1.91}_{-0.63}$	$15.47^{+4.82}_{-4.20}$	$17.40^{+4.82}_{-4.20}$	$20.32^{+0.64}_{-0.37}$	74.5	86.8
		M2021	$1.56^{+1.22}_{-0.73}$	$4.50^{+6.42}_{-2.73}$	$10.54^{+3.22}_{-1.89}$	$12.47^{+3.22}_{-1.89}$		98.0	99.3
		$\sim M^{-1}$	$1.68^{+1.28}_{-0.81}$	$3.68^{+5.80}_{-2.35}$	$11.02^{+4.06}_{-2.16}$	$12.95^{+4.06}_{-2.16}$		94.2	97.0
270	3.60	K2001	$1.95^{+1.00}_{-0.71}$	$0.50^{+0.30}_{-0.24}$	$20.28^{+3.05}_{-3.69}$	$23.88^{+3.05}_{-3.69}$	$23.89^{+1.11}_{-0.92}$	49.0	88.4
		M2021	$1.20^{+0.85}_{-0.55}$	$0.90^{+0.81}_{-0.43}$	$15.72^{+4.80}_{-4.28}$	$19.32^{+4.80}_{-4.28}$		82.0	98.2
		$\sim M^{-1}$	$1.80^{+1.04}_{-0.86}$	$0.52^{+0.61}_{-0.25}$	$19.88^{+3.19}_{-5.88}$	$23.48^{+3.19}_{-5.88}$		54.3	90.1
284	4.43	K2001	$1.16^{+0.28}_{-0.30}$	$0.10^{+0.04}_{-0.02}$	$19.88^{+3.19}_{-5.88}$	$29.09^{+1.71}_{-1.91}$	25.00	1.3	58.9
		M2021	$1.25^{+0.55}_{-0.45}$	$0.09^{+0.06}_{-0.03}$	$25.16^{+3.38}_{-2.96}$	$29.59^{+3.38}_{-2.96}$		3.3	48.7
		$\sim M^{-1}$	$1.58^{+0.53}_{-0.50}$	$0.07^{+0.04}_{-0.02}$	$28.24^{+0.65}_{-4.07}$	$32.67^{+0.65}_{-4.07}$		1.2	24.3
326	4.35	K2001	$1.54^{+1.33}_{-0.70}$	$1.12^{+1.26}_{-0.64}$	$15.03^{+6.05}_{-4.53}$	$19.38^{+6.05}_{-4.53}$	$24.51^{+0.49}_{-1.03}$	79.5	88.0
		M2021	$0.86^{+0.59}_{-0.31}$	$2.40^{+1.56}_{-1.13}$	$10.49^{+3.77}_{-2.18}$	$14.83^{+3.77}_{-2.18}$		98.9	99.8
		$\sim M^{-1}$	$0.96^{+0.82}_{-0.38}$	$2.09^{+1.66}_{-1.13}$	$11.09^{+5.03}_{-2.54}$	$15.44^{+5.03}_{-2.54}$		92.8	95.8

Table 1. Continued.

<i>Gaia</i> DR3- ULENS	A_G [mag]	MF	D_L [kpc]	M_L [M_\odot]	$G_{MS,0}$ [mag]	$G_{MS,A}$ [mag]	G_{blend} [mag]	P_A [%]	P_0 [%]
343	2.22	K2001	$1.54^{+0.70}_{-0.57}$	$0.65^{+0.47}_{-0.25}$	$18.44^{+3.02}_{-4.36}$	$20.66^{+3.02}_{-4.36}$	25.00	92.3	98.4
		M2021	$0.95^{+0.55}_{-0.42}$	$1.15^{+1.02}_{-0.48}$	$13.88^{+4.14}_{-4.24}$	$16.10^{+4.14}_{-4.24}$		99.1	99.9
		$\sim M^{-1}$	$1.24^{+0.84}_{-0.59}$	$0.85^{+0.91}_{-0.40}$	$16.18^{+4.67}_{-4.82}$	$18.40^{+4.67}_{-4.82}$		94.4	99.0
353	0.08	K2001	$2.12^{+0.83}_{-0.77}$	$0.75^{+0.58}_{-0.33}$	$18.07^{+3.77}_{-4.00}$	$18.15^{+3.77}_{-4.00}$	$24.08^{+0.92}_{-1.11}$	94.8	95.1
		M2021	$1.49^{+0.71}_{-0.67}$	$1.34^{+1.01}_{-0.50}$	$14.09^{+3.26}_{-3.48}$	$14.17^{+3.26}_{-3.48}$		99.7	99.8
		$\sim M^{-1}$	$1.68^{+0.92}_{-0.75}$	$1.14^{+0.94}_{-0.52}$	$15.16^{+4.50}_{-3.97}$	$15.24^{+4.50}_{-3.97}$		98.3	98.4
363	7.63	K2001	$1.61^{+0.82}_{-0.62}$	$0.59^{+0.41}_{-0.26}$	$18.97^{+3.23}_{-4.20}$	$26.61^{+3.23}_{-4.20}$	$23.90^{+1.10}_{-0.93}$	25.5	94.0
		M2021	$1.03^{+0.65}_{-0.46}$	$1.07^{+0.86}_{-0.46}$	$14.42^{+4.44}_{-3.86}$	$22.05^{+4.44}_{-3.86}$		66.4	99.4
		$\sim M^{-1}$	$1.61^{+0.82}_{-0.61}$	$0.59^{+0.42}_{-0.26}$	$18.94^{+3.24}_{-4.19}$	$26.57^{+3.24}_{-4.19}$		25.7	94.1

Table A.1. Table of the results of cross-match between 204 analysed *Gaia* DR3 events with other surveys.

<i>Gaia</i> DR3- ULENS-	RA [deg]	Dec [deg]	Remarks
002	258.0717	-16.8677	AP29744086
003	284.4367	-20.7758	AP28506888
007	270.2540	-32.6896	OGLE-2015-BLG-0064 AP27808437
013	274.7611	-27.7294	OGLE-2015-BLG-1755
...
363	266.9194	-25.0204	BLG633.01.52040 OGLE-2017-BLG-0116 KMT-2017-BLG-1029

Appendix A: Additional tables

In this appendix, we provide three tables:

- Table A.1, which is the result of the cross-match between the preliminary sample of 204 *Gaia* DR3 microlensing events and other surveys;
- Table A.2, which is the list of data sets used to obtain the final models for each of the 35 analysed events;
- Table A.3, which is the list of parameters of best-fitting solutions of the 35 analysed events. In this paper, the baseline magnitude and blending parameter are only provided for the *G*-band. A full, machine-readable version of this table, with all parameters, is available online.

Table A.2. The list of data sets used to obtain the final models for each of the 35 analysed events.

<i>Gaia</i> DR3- ULENS-	Survey, filter	Num. of points	<i>Gaia</i> DR3- ULENS-	Survey, filter	Num. of points
003	<i>Gaia, G</i>	27	018	<i>Gaia, G</i>	24
	<i>Gaia, G_{BP}</i>	27		OGLE, I	537
	<i>Gaia, G_{RP}</i>	27			
	ASASSN, V	84			
023	<i>Gaia, G</i>	64	025	<i>Gaia, G</i>	33
	<i>Gaia, G_{BP}</i>	60		<i>Gaia, G_{RP}</i>	32
	<i>Gaia, G_{RP}</i>	60		OGLE, I	99
	OGLE, I	125			
	ASASSN, V	410			
032	<i>Gaia, G</i>	40	035	<i>Gaia, G</i>	6
	<i>Gaia, G_{BP}</i>	38		<i>Gaia, G_{RP}</i>	5
	<i>Gaia, G_{RP}</i>	37		OGLE, I	371
	ASASSN, V	307		MOA	3448
047	<i>Gaia, G</i>	21	057	<i>Gaia, G</i>	24
	<i>Gaia, G_{RP}</i>	10		<i>Gaia, G_{RP}</i>	23
	KMTNet SAAO, I	804			
	KMTNet CTIO, I	363			
KMTNet SSO, I	720				
069	<i>Gaia, G</i>	36	073	<i>Gaia, G</i>	22
	<i>Gaia, G_{RP}</i>	30		<i>Gaia, G_{RP}</i>	13
	KMTNet SAAO, I	731		OGLE, I	604
	KMTNet CTIO, I	831		MOA	6102
	KMTNet SSO, I	731			
MOA	29814				
078	<i>Gaia, G</i>	40	079	<i>Gaia, G</i>	24
	<i>Gaia, G_{BP}</i>	39		<i>Gaia, G_{RP}</i>	22
	<i>Gaia, G_{RP}</i>	39		OGLE, I	1255
	OGLE, I	634		KMTNet SAAO, I	2010
			KMTNet CTIO, I	4314	
			KMTNet SSO, I	2669	
			MOA	9285	
088	<i>Gaia, G</i>	33	089	<i>Gaia, G</i>	25
	OGLE, I	1678		OGLE, I	609
	KMTNet SAAO, I	511		KMTNet SAAO, I	249
	KMTNet CTIO, I	819		KMTNet CTIO, I	395
	KMTNet SSO, I	730		KMTNet SSO, I	348
MOA	24908				
097	<i>Gaia, G</i>	54	103	<i>Gaia, G</i>	66
	<i>Gaia, G_{RP}</i>	52		<i>Gaia, G_{BP}</i>	59
	OGLE, I	543		<i>Gaia, G_{RP}</i>	63
			OGLE, I	143	
118	<i>Gaia, G</i>	22	127	<i>Gaia, G</i>	25
	<i>Gaia, G_{RP}</i>	20		OGLE, I	1918
	OGLE, I	166		KMTNet SAAO, I	285
	ASASSN, V	19		KMTNet CTIO, I	412
			KMTNet SSO, I	382	
142	<i>Gaia, G</i>	29	143	<i>Gaia, G</i>	60
	<i>Gaia, G_{RP}</i>	25		OGLE, I	122
			OGLE, I	274	

Table A.2. continued.

<i>Gaia</i> DR3- ULENS-	Survey, filter	Num. of points	<i>Gaia</i> DR3- ULENS-	Survey, filter	Num. of points
155	<i>Gaia, G</i>	47	196	<i>Gaia, G</i>	60
	<i>Gaia, G_{RP}</i>	44		<i>Gaia, G_{RP}</i>	56
	OGLE, I	1347		OGLE, I	572
	KMTNet SAAO, I	216			
	KMTNet CTIO, I	379			
	KMTNet SSO, I	324			
	MOA	3290			
212	<i>Gaia, G</i>	59	230	<i>Gaia, G</i>	28
	GSA, <i>G</i>	68		OGLE, I	1985
	OGLE, I	189			
	KMTNet SAAO, I	706			
	KMTNet CTIO, I	971			
	KMTNet SSO, I	867			
259	<i>Gaia, G</i>	58	270	<i>Gaia, G</i>	24
	<i>Gaia, G_{RP}</i>	50		OGLE, I	778
	GSA, <i>G</i>	164		KMTNet SAAO, I	568
	OGLE, I	52		KMTNet CTIO, I	859
			KMTNet SSO, I	778	
275	<i>Gaia, G</i>	40	284	<i>Gaia, G</i>	42
	<i>Gaia, G_{RP}</i>	39		OGLE, I	643
	OGLE, I	130		KMTNet SAAO, I	640
			KMTNet CTIO, I	992	
			KMTNet SSO, I	888	
326	<i>Gaia, G</i>	39	331	<i>Gaia, G</i>	42
	OGLE, I	1625		OGLE, I	843
	KMTNet SAAO, I	538		KMTNet SAAO, I	549
	KMTNet CTIO, I	827		KMTNet CTIO, I	549
	KMTNet SSO, I	746	KMTNet SSO, I	768	
343	<i>Gaia, G</i>	20	353	<i>Gaia, G</i>	18
	<i>Gaia, G_{RP}</i>	9		<i>Gaia, G_{RP}</i>	11
	OGLE, I	1685		OGLE, I	742
	KMTNet SAAO, I	650		KMTNet SAAO, I	625
	KMTNet CTIO, I	908		KMTNet SSO, I	800
	KMTNet SSO, I	835		MOA	3066
	MOA	15768			
359	<i>Gaia, G</i>	21	363	<i>Gaia, G</i>	23
	OGLE, I	486		OGLE, I	457
	KMTNet SAAO, I	212		KMTNet SAAO, I	758
	KMTNet CTIO, I	382		KMTNet CTIO, I	1026
	KMTNet SSO, I	343	KMTNet SSO, I	928	

Table A.3. Parameters of all best-fitting solutions of the 35 analysed events. The table contains parameters for two types of microlensing point source-point lens models: with and without parallax. The non-parallax PSPL model parameters are: t_0 – the time of the peak of brightness, u_0 – corresponding separation of the lens and source at t_0 , t_E – Einstein timescale of the event, $I_{0,G}$ – brightness in baseline in the *G*-band, $f_{b,G}$ – a fraction of the total flux at baseline belonging to the blend in the *G*-band. The parallax model adds two additional parameters: π_{EN} and π_{EE} , which are north and east components of the microlensing parallax vector. $t_{0,par}$ is a non-fitted parameter, which defines the coordinate system for parallax measurement. Both t_0 and $t_{0,par}$ are in $HJD' = HJD - 2450000$.

<i>Gaia</i> DR3- ULENS-	$t_{0,par}$	t_0	u_0	t_E	π_{EN}	π_{EE}	$I_{0,G}$	$f_{b,G}$	χ^2
003-G0	–	7297.84 ^{+0.11} _{–0.11}	0.05 ^{+0.01} _{–0.01}	64.90 ^{+4.60} _{–4.48}	–	–	14.16 ^{+0.01} _{–0.01}	0.25 ^{+0.07} _{–0.08}	262.7
003-G-1		7298.61 ^{+0.32} _{–0.32}	–0.05 ^{+0.01} _{–0.01}	63.04 ^{+12.98} _{–12.98}	–0.49 ^{+0.30} _{–0.30}	0.17 ^{+0.07} _{–0.07}	14.16 ^{+0.01} _{–0.01}	0.20 ^{+0.17} _{–0.17}	322.9
003-G-2	7297.0	7298.48 ^{+0.29} _{–0.29}	–0.04 ^{+0.01} _{–0.01}	62.96 ^{+14.72} _{–14.72}	0.42 ^{+0.26} _{–0.26}	0.08 ^{+0.07} _{–0.07}	14.16 ^{+0.01} _{–0.01}	0.22 ^{+0.20} _{–0.20}	353.9
003-G+1		7298.53 ^{+0.30} _{–0.30}	0.04 ^{+0.01} _{–0.01}	62.18 ^{+11.10} _{–11.10}	–0.46 ^{+0.30} _{–0.30}	0.17 ^{+0.07} _{–0.07}	14.16 ^{+0.01} _{–0.01}	0.21 ^{+0.16} _{–0.16}	388.3
003-G+2		7298.54 ^{+0.30} _{–0.30}	0.05 ^{+0.01} _{–0.01}	63.61 ^{+12.50} _{–12.50}	0.44 ^{+0.24} _{–0.24}	0.09 ^{+0.07} _{–0.07}	14.16 ^{+0.01} _{–0.01}	0.21 ^{+0.16} _{–0.16}	294.2
018-G0	–	7721.35 ^{+0.23} _{–0.22}	0.66 ^{+0.08} _{–0.07}	95.63 ^{+5.57} _{–5.70}	–	–	15.99 ^{+0.00} _{–0.00}	0.48 ^{+0.08} _{–0.11}	652.3
018-G+	7720.0	7712.05 ^{+1.65} _{–1.68}	0.15 ^{+0.08} _{–0.04}	371.66 ^{+143.35} _{–128.09}	–0.05 ^{+0.03} _{–0.01}	–0.10 ^{+0.02} _{–0.01}	16.00 ^{+0.00} _{–0.00}	0.94 ^{+0.02} _{–0.04}	550.9
018-G-		7716.08 ^{+1.88} _{–2.62}	–0.14 ^{+0.01} _{–0.01}	348.49 ^{+47.22} _{–41.66}	0.14 ^{+0.03} _{–0.03}	–0.05 ^{+0.02} _{–0.02}	16.00 ^{+0.00} _{–0.00}	0.94 ^{+0.01} _{–0.01}	546.4
023-G0	–	7726.46 ^{+0.08} _{–0.08}	0.01 ^{+0.01} _{–0.01}	489.25 ^{+16.06} _{–15.26}	–	–	16.05 ^{+0.01} _{–0.01}	0.86 ^{+0.01} _{–0.01}	2350.4
023-G+	7724.0	7725.98 ^{+0.09} _{–0.09}	0.03 ^{+0.01} _{–0.01}	134.66 ^{+5.84} _{–5.61}	–0.05 ^{+0.01} _{–0.01}	0.16 ^{+0.01} _{–0.01}	16.00 ^{+0.01} _{–0.01}	0.40 ^{+0.03} _{–0.03}	359.3
023-G-		7725.97 ^{+0.08} _{–0.08}	–0.03 ^{+0.01} _{–0.01}	131.76 ^{+5.89} _{–5.49}	–0.05 ^{+0.01} _{–0.01}	0.16 ^{+0.01} _{–0.01}	16.00 ^{+0.01} _{–0.01}	0.39 ^{+0.03} _{–0.03}	363.3
025-G0	–	7491.54 ^{+0.33} _{–0.32}	0.20 ^{+0.01} _{–0.01}	108.86 ^{+2.10} _{–2.07}	–	–	16.13 ^{+0.01} _{–0.01}	0.01 ^{+0.01} _{–0.01}	519.8
025-G+ v 025-G-	7491.0	7487.23 ^{+0.87} _{–1.43} 7488.75 ^{+0.43} _{–0.42}	0.12 ^{+0.01} _{–0.01} –0.19 ^{+0.01} _{–0.01}	176.68 ^{+17.00} _{–14.87} 112.45 ^{+5.67} _{–4.19}	0.60 ^{+0.13} _{–0.10} –0.67 ^{+0.11} _{–0.11}	0.31 ^{+0.11} _{–0.07} 0.16 ^{+0.04} _{–0.04}	16.12 ^{+0.01} _{–0.01} 16.12 ^{+0.01} _{–0.01}	0.45 ^{+0.07} _{–0.08} 0.05 ^{+0.06} _{–0.04}	172.1 173.6
032-G0	–	7022.95 ^{+0.10} _{–0.11}	0.00 ^{+0.01} _{–0.01}	52.93 ^{+4.27} _{–3.51}	–	–	16.33 ^{+0.01} _{–0.01}	0.24 ^{+0.12} _{–0.12}	1333.3
032-G+	7015.0	7022.98 ^{+0.15} _{–0.16}	–0.01 ^{+0.02} _{–0.02}	49.35 ^{+3.32} _{–2.69}	1.03 ^{+0.19} _{–0.26}	–0.79 ^{+0.40} _{–0.33}	16.33 ^{+0.01} _{–0.01}	0.17 ^{+0.13} _{–0.11}	1322.5
032-G-		7021.78 ^{+0.29} _{–0.30}	0.01 ^{+0.01} _{–0.01}	524.04 ^{+572.35} _{–226.99}	–0.76 ^{+0.37} _{–0.44}	–0.01 ^{+0.07} _{–0.03}	16.33 ^{+0.01} _{–0.01}	0.93 ^{+0.04} _{–0.07}	1347.9
035-G0	–	7090.19 ^{+0.01} _{–0.01}	0.08 ^{+0.01} _{–0.01}	58.91 ^{+0.10} _{–0.10}	–	–	16.46 ^{+0.01} _{–0.01}	0.06 ^{+0.01} _{–0.01}	1246.1
035-G+	7090.0	7090.18 ^{+0.01} _{–0.01}	0.08 ^{+0.01} _{–0.01}	58.36 ^{+0.40} _{–0.40}	0.02 ^{+0.02} _{–0.02}	0.01 ^{+0.01} _{–0.01}	16.46 ^{+0.01} _{–0.01}	0.05 ^{+0.01} _{–0.01}	1243.4
035-G-		7090.18 ^{+0.01} _{–0.01}	–0.08 ^{+0.01} _{–0.01}	58.45 ^{+0.42} _{–0.42}	0.02 ^{+0.03} _{–0.03}	0.01 ^{+0.01} _{–0.01}	16.46 ^{+0.01} _{–0.01}	0.05 ^{+0.01} _{–0.01}	1243.4
047-G0	–	7265.84 ^{+0.01} _{–0.01}	0.09 ^{+0.01} _{–0.01}	85.95 ^{+0.04} _{–0.04}	–	–	16.63 ^{+0.01} _{–0.01}	0.01 ^{+0.01} _{–0.01}	5698.1
047-G+	7264.0	7265.88 ^{+0.01} _{–0.01}	0.09 ^{+0.01} _{–0.01}	87.23 ^{+0.19} _{–0.12}	–0.02 ^{+0.01} _{–0.01}	0.21 ^{+0.01} _{–0.01}	16.63 ^{+0.01} _{–0.01}	0.01 ^{+0.01} _{–0.01}	722797.7
047-G-		7265.72 ^{+0.01} _{–0.01}	–0.09 ^{+0.01} _{–0.01}	85.52 ^{+0.06} _{–0.05}	–0.02 ^{+0.01} _{–0.01}	0.27 ^{+0.01} _{–0.01}	16.63 ^{+0.01} _{–0.01}	0.00 ^{+0.01} _{–0.01}	1381574.6
057-G0	–	7443.92 ^{+7.02} _{–4.99}	0.10 ^{+0.06} _{–0.04}	82.94 ^{+43.52} _{–17.63}	–	–	16.80 ^{+0.01} _{–0.01}	0.52 ^{+0.27} _{–0.33}	12.0
069-G0	–	7328.34 ^{+0.04} _{–0.04}	0.13 ^{+0.01} _{–0.01}	106.69 ^{+0.21} _{–0.21}	–	–	17.07 ^{+0.01} _{–0.01}	0.22 ^{+0.01} _{–0.01}	85286.9
069-G+	7328.0	7329.97 ^{+0.05} _{–0.06}	0.15 ^{+0.01} _{–0.01}	94.66 ^{+0.36} _{–0.20}	0.03 ^{+0.01} _{–0.01}	0.03 ^{+0.01} _{–0.01}	17.07 ^{+0.01} _{–0.01}	0.01 ^{+0.01} _{–0.01}	84875.0
069-G-		7329.52 ^{+0.09} _{–0.09}	–0.14 ^{+0.01} _{–0.01}	103.47 ^{+0.74} _{–0.75}	–0.07 ^{+0.01} _{–0.01}	0.02 ^{+0.01} _{–0.01}	17.07 ^{+0.01} _{–0.01}	0.15 ^{+0.01} _{–0.01}	84872.9

Table A.3. continued.

<i>Gaia</i> DR3- ULENS-	$t_{0,\text{par}}$	t_0	u_0	t_E	π_{EN}	π_{EE}	$l_{0,G}$	$f_{b,G}$	χ^2
073-G0	–	7406.87 ^{+0.12} _{–0.12}	0.34 ^{+0.01} _{–0.01}	113.36 ^{+0.52} _{–0.31}	–	–	17.14 ^{+0.01} _{–0.01}	0.01 ^{+0.01} _{–0.01}	16428.0
073-G-	7406.00	7409.12 ^{+0.53} _{–0.52}	–0.27 ^{+0.02} _{–0.02}	137.44 ^{+8.32} _{–8.07}	–0.03 ^{+0.01} _{–0.01}	–0.02 ^{+0.02} _{–0.02}	17.14 ^{+0.01} _{–0.01}	0.29 ^{+0.07} _{–0.08}	16655.2
078-G0	–	6956.49 ^{+1.91} _{–1.33}	0.30 ^{+0.11} _{–0.07}	47.48 ^{+7.53} _{–7.21}	–	–	17.19 ^{+0.01} _{–0.01}	0.82 ^{+0.05} _{–0.10}	7625.9
078-G+	6956.0	6957.47 ^{+2.04} _{–1.71}	0.52 ^{+0.30} _{–0.17}	33.53 ^{+10.07} _{–7.88}	0.50 ^{+0.27} _{–0.29}	0.55 ^{+0.33} _{–0.37}	17.19 ^{+0.01} _{–0.01}	0.61 ^{+0.18} _{–0.47}	1228.8
078-G-		6957.57 ^{+2.98} _{–1.87}	–0.55 ^{+0.23} _{–0.40}	31.65 ^{+13.99} _{–7.99}	0.52 ^{+0.31} _{–0.33}	–0.50 ^{+0.32} _{–0.30}	17.19 ^{+0.01} _{–0.01}	0.57 ^{+0.24} _{–0.75}	1268.8
079-G0	–	7301.46 ^{+0.02} _{–0.02}	0.25 ^{+0.01} _{–0.01}	105.19 ^{+0.30} _{–0.30}	–	–	17.23 ^{+0.01} _{–0.01}	0.50 ^{+0.01} _{–0.01}	112941.8
079-G+	7301.0	7301.30 ^{+0.02} _{–0.02}	0.15 ^{+0.01} _{–0.01}	167.12 ^{+1.33} _{–1.30}	–0.04 ^{+0.01} _{–0.01}	–0.09 ^{+0.01} _{–0.01}	17.24 ^{+0.01} _{–0.01}	0.72 ^{+0.01} _{–0.01}	106429.7
079-G-		7301.33 ^{+0.02} _{–0.02}	–0.16 ^{+0.00} _{–0.00}	160.41 ^{+0.86} _{–0.84}	0.02 ^{+0.01} _{–0.01}	–0.09 ^{+0.01} _{–0.01}	17.24 ^{+0.01} _{–0.01}	0.70 ^{+0.01} _{–0.01}	106538.9
088-G0	–	7668.80 ^{+0.05} _{–0.05}	0.54 ^{+0.01} _{–0.01}	106.76 ^{+0.09} _{–0.08}	–	–	17.35 ^{+0.01} _{–0.01}	0.00 ^{+0.01} _{–0.01}	79806.6
088-G+	7668.0	7668.74 ^{+0.09} _{–0.09}	0.47 ^{+0.01} _{–0.01}	114.85 ^{+1.77} _{–1.76}	–0.05 ^{+0.01} _{–0.01}	–0.02 ^{+0.01} _{–0.01}	17.35 ^{+0.01} _{–0.01}	0.18 ^{+0.03} _{–0.03}	79523.9
088-G-		7668.82 ^{+0.08} _{–0.08}	–0.51 ^{+0.01} _{–0.01}	105.41 ^{+0.62} _{–0.62}	0.08 ^{+0.01} _{–0.01}	–0.01 ^{+0.01} _{–0.01}	17.35 ^{+0.01} _{–0.01}	0.08 ^{+0.02} _{–0.02}	79435.5
089-G0	–	7645.86 ^{+0.01} _{–0.01}	0.32 ^{+0.01} _{–0.01}	70.61 ^{+0.04} _{–0.04}	–	–	17.37 ^{+0.01} _{–0.01}	0.00 ^{+0.01} _{–0.01}	11769.1
089-G+	7645.0	7645.21 ^{+0.02} _{–0.02}	0.25 ^{+0.01} _{–0.01}	77.40 ^{+2.09} _{–1.85}	–0.45 ^{+0.03} _{–0.03}	–0.09 ^{+0.01} _{–0.01}	17.38 ^{+0.01} _{–0.01}	0.24 ^{+0.04} _{–0.04}	6587.5
089-G-1		7645.32 ^{+0.02} _{–0.02}	–0.32 ^{+0.01} _{–0.01}	77.07 ^{+2.25} _{–1.50}	–0.25 ^{+0.05} _{–0.05}	–0.13 ^{+0.01} _{–0.01}	17.38 ^{+0.01} _{–0.01}	0.02 ^{+0.02} _{–0.01}	6690.8
089-G-2		7645.22 ^{+0.02} _{–0.02}	–0.27 ^{+0.01} _{–0.01}	73.25 ^{+1.40} _{–1.29}	0.45 ^{+0.03} _{–0.03}	–0.10 ^{+0.01} _{–0.01}	17.38 ^{+0.01} _{–0.01}	0.17 ^{+0.03} _{–0.03}	6620.7
097-G0	–	7782.71 ^{+1.27} _{–1.22}	0.28 ^{+0.04} _{–0.04}	111.51 ^{+8.57} _{–8.03}	–	–	17.43 ^{+0.01} _{–0.01}	0.84 ^{+0.03} _{–0.03}	643.8
097-G+	7782.00	7769.75 ^{+2.11} _{–1.88}	0.69 ^{+0.09} _{–0.15}	54.44 ^{+8.32} _{–4.39}	0.22 ^{+0.05} _{–0.05}	0.26 ^{+0.10} _{–0.10}	17.43 ^{+0.00} _{–0.00}	0.28 ^{+0.24} _{–0.19}	637.0
103-G0	–	7788.97 ^{+0.30} _{–0.30}	0.05 ^{+0.01} _{–0.01}	65.46 ^{+2.77} _{–2.58}	–	–	17.56 ^{+0.01} _{–0.01}	0.05 ^{+0.07} _{–0.08}	145.8
103-G+	7788.0	7789.01 ^{+0.30} _{–0.29}	0.06 ^{+0.01} _{–0.01}	58.03 ^{+6.75} _{–5.55}	0.13 ^{+0.10} _{–0.08}	–0.03 ^{+0.29} _{–0.32}	17.55 ^{+0.01} _{–0.01}	–0.12 ^{+0.17} _{–0.17}	176.4
103-G-		7789.01 ^{+0.29} _{–0.29}	–0.06 ^{+0.01} _{–0.01}	57.96 ^{+7.51} _{–5.95}	0.13 ^{+0.11} _{–0.08}	–0.02 ^{+0.31} _{–0.36}	17.55 ^{+0.01} _{–0.01}	–0.11 ^{+0.16} _{–0.17}	177.5
118-G0	–	7668.88 ^{+0.18} _{–0.17}	0.04 ^{+0.01} _{–0.00}	79.89 ^{+3.28} _{–3.19}	–	–	17.73 ^{+0.00} _{–0.00}	0.20 ^{+0.04} _{–0.04}	232.0
118-G+	7669.0	7668.30 ^{+0.20} _{–0.20}	0.04 ^{+0.01} _{–0.01}	76.20 ^{+14.97} _{–7.13}	0.75 ^{+0.06} _{–0.06}	0.61 ^{+0.11} _{–0.12}	17.72 ^{+0.01} _{–0.01}	0.16 ^{+0.16} _{–0.11}	177.8
118-G-		7668.08 ^{+0.22} _{–0.22}	–0.04 ^{+0.01} _{–0.01}	84.40 ^{+20.45} _{–10.78}	0.75 ^{+0.05} _{–0.06}	0.65 ^{+0.13} _{–0.14}	17.72 ^{+0.01} _{–0.01}	0.21 ^{+0.17} _{–0.14}	177.3
127-G0	–	7851.17 ^{+0.08} _{–0.08}	0.33 ^{+0.01} _{–0.01}	106.71 ^{+2.39} _{–2.35}	–	–	17.88 ^{+0.01} _{–0.01}	0.69 ^{+0.01} _{–0.01}	10516.4
127-G+	7851.0	7851.17 ^{+0.13} _{–0.14}	0.34 ^{+0.02} _{–0.02}	106.92 ^{+3.81} _{–3.61}	–0.03 ^{+0.06} _{–0.05}	–0.01 ^{+0.01} _{–0.01}	17.88 ^{+0.01} _{–0.01}	0.68 ^{+0.03} _{–0.03}	10516.6
127-G-		7851.20 ^{+0.12} _{–0.13}	–0.33 ^{+0.02} _{–0.02}	108.57 ^{+3.66} _{–3.54}	0.02 ^{+0.06} _{–0.08}	–0.01 ^{+0.01} _{–0.01}	17.88 ^{+0.01} _{–0.01}	0.70 ^{+0.02} _{–0.02}	10517.2
142-G0	–	7289.94 ^{+0.38} _{–0.37}	0.58 ^{+0.01} _{–0.01}	112.65 ^{+0.67} _{–0.57}	–	–	18.03 ^{+0.01} _{–0.01}	0.01 ^{+0.01} _{–0.01}	1099.6
142-G+1		7285.29 ^{+0.55} _{–0.56}	0.26 ^{+0.02} _{–0.02}	181.28 ^{+11.83} _{–11.89}	–0.19 ^{+0.01} _{–0.01}	–0.05 ^{+0.01} _{–0.01}	18.03 ^{+0.01} _{–0.01}	0.66 ^{+0.03} _{–0.04}	702.0
142-G+2	7289.0	7281.39 ^{+1.06} _{–1.13}	0.54 ^{+0.02} _{–0.03}	124.24 ^{+3.44} _{–3.24}	0.02 ^{+0.04} _{–0.04}	–0.08 ^{+0.01} _{–0.01}	18.03 ^{+0.01} _{–0.01}	0.06 ^{+0.08} _{–0.04}	719.3

Table A.3. continued.

<i>Gaia</i> DR3- ULENS-	$t_{0,\text{par}}$	t_0	u_0	t_E	π_{EN}	π_{EE}	$l_{0,G}$	$f_{b,G}$	χ^2
142-G-1		7285.36 ^{+0.53} _{-0.59}	-0.28 ^{+0.02} _{-0.03}	169.24 ^{+11.10} _{-11.11}	0.21 ^{+0.01} _{-0.02}	-0.03 ^{+0.01} _{-0.01}	18.03 ^{+0.01} _{-0.01}	0.63 ^{+0.04} _{-0.05}	703.6
142-G-2		7280.76 ^{+1.24} _{-1.36}	-0.54 ^{+0.02} _{-0.01}	126.62 ^{+5.38} _{-4.13}	-0.04 ^{+0.05} _{-0.04}	-0.08 ^{+0.01} _{-0.01}	18.03 ^{+0.01} _{-0.01}	0.04 ^{+0.07} _{-0.03}	716.2
143-G0	–	7048.69 ^{+2.78} _{-2.50}	0.07 ^{+0.08} _{-0.05}	67.15 ^{+2.59} _{-2.44}	–	–	18.03 ^{+0.01} _{-0.01}	0.06 ^{+0.09} _{-0.05}	131.0
143-G+	7048.0	7051.53 ^{+12.36} _{-9.16}	0.17 ^{+0.13} _{-0.10}	111.94 ^{+55.53} _{-25.64}	0.28 ^{+0.27} _{-0.41}	-0.21 ^{+0.15} _{-0.10}	18.03 ^{+0.01} _{-0.01}	0.51 ^{+0.24} _{-0.33}	107.7
143-G+2		7061.30 ^{+8.37} _{-7.22}	0.22 ^{+0.12} _{-0.12}	66.65 ^{+12.54} _{-6.65}	0.28 ^{+0.17} _{-0.29}	-0.35 ^{+0.09} _{-0.11}	18.03 ^{+0.01} _{-0.01}	0.35 ^{+0.27} _{-0.24}	107.9
155-G0	–	7437.60 ^{+0.04} _{-0.04}	0.10 ^{+0.01} _{-0.01}	66.23 ^{+0.35} _{-0.35}	–	–	18.13 ^{+0.01} _{-0.01}	0.21 ^{+0.01} _{-0.01}	13511.8
155-G+	7437.0	7437.57 ^{+0.05} _{-0.05}	0.10 ^{+0.00} _{-0.00}	63.17 ^{+1.68} _{-1.73}	0.19 ^{+0.04} _{-0.04}	0.03 ^{+0.02} _{-0.02}	18.13 ^{+0.01} _{-0.01}	0.18 ^{+0.03} _{-0.03}	13495.8
155-G-		7437.59 ^{+0.05} _{-0.05}	-0.10 ^{+0.01} _{-0.01}	64.10 ^{+1.62} _{-1.71}	0.22 ^{+0.04} _{-0.05}	0.04 ^{+0.03} _{-0.02}	18.13 ^{+0.01} _{-0.01}	0.17 ^{+0.03} _{-0.03}	13496.5
196-G0	–	7356.19 ^{+1.10} _{-1.20}	0.32 ^{+0.12} _{-0.18}	64.71 ^{+5.13} _{-3.91}	–	–	18.48 ^{+0.01} _{-0.01}	0.23 ^{+0.17} _{-0.16}	643.7
196-G+	7356.0	7358.74 ^{+5.29} _{-9.33}	0.20 ^{+0.23} _{-0.13}	114.62 ^{+58.96} _{-33.10}	-0.12 ^{+0.25} _{-0.14}	-0.35 ^{+0.25} _{-0.24}	18.49 ^{+0.01} _{-0.01}	0.65 ^{+0.16} _{-0.32}	691.5
196-G-		7351.48 ^{+5.25} _{-8.89}	-0.40 ^{+0.13} _{-0.16}	105.80 ^{+55.57} _{-30.21}	0.32 ^{+0.30} _{-0.30}	-0.15 ^{+0.29} _{-0.15}	18.49 ^{+0.01} _{-0.01}	0.51 ^{+0.22} _{-0.32}	633.1
212-G0	–	7879.01 ^{+0.01} _{-0.01}	0.16 ^{+0.01} _{-0.01}	55.77 ^{+0.15} _{-0.15}	–	–	18.38 ^{+0.01} _{-0.01}	-0.01 ^{+0.01} _{-0.01}	15998.7
212-G+	7879.0	7879.05 ^{+0.01} _{-0.01}	0.16 ^{+0.01} _{-0.01}	55.72 ^{+0.15} _{-0.15}	-0.03 ^{+0.03} _{-0.03}	-0.04 ^{+0.01} _{-0.01}	18.38 ^{+0.01} _{-0.01}	-0.02 ^{+0.01} _{-0.01}	15608.8
212-G-		7879.05 ^{+0.01} _{-0.01}	-0.16 ^{+0.01} _{-0.01}	55.51 ^{+0.18} _{-0.18}	-0.03 ^{+0.03} _{-0.03}	-0.04 ^{+0.01} _{-0.01}	18.38 ^{+0.01} _{-0.01}	-0.02 ^{+0.01} _{-0.01}	15609.5
212-GSA0	–	7879.01 ^{+0.01} _{-0.01}	0.16 ^{+0.01} _{-0.01}	55.77 ^{+0.15} _{-0.15}	–	–	18.43 ^{+0.01} _{-0.01}	-0.03 ^{+0.01} _{-0.01}	16041.2
212-GSA+	7879.0	7879.05 ^{+0.01} _{-0.01}	0.16 ^{+0.01} _{-0.01}	55.72 ^{+0.15} _{-0.15}	-0.03 ^{+0.03} _{-0.03}	-0.04 ^{+0.01} _{-0.01}	18.44 ^{+0.01} _{-0.01}	-0.04 ^{+0.01} _{-0.01}	15650.5
212-GSA-		7879.05 ^{+0.01} _{-0.01}	-0.16 ^{+0.01} _{-0.01}	55.50 ^{+0.19} _{-0.18}	-0.03 ^{+0.03} _{-0.03}	-0.04 ^{+0.01} _{-0.01}	18.44 ^{+0.01} _{-0.01}	-0.04 ^{+0.01} _{-0.01}	15650.9
230-G0	–	7123.59 ^{+0.39} _{-0.39}	0.80 ^{+0.23} _{-0.22}	24.42 ^{+5.23} _{-3.64}	–	–	18.72 ^{+0.01} _{-0.01}	0.53 ^{+0.19} _{-0.30}	2696.4
230-G+	7123.0	7122.70 ^{+0.45} _{-0.45}	0.88 ^{+0.29} _{-0.23}	22.89 ^{+4.73} _{-3.80}	0.83 ^{+0.12} _{-0.19}	-0.27 ^{+0.79} _{-0.53}	18.72 ^{+0.01} _{-0.01}	0.43 ^{+0.24} _{-0.47}	2719.6
230-G-		7122.72 ^{+0.43} _{-0.44}	-0.87 ^{+0.23} _{-0.33}	23.03 ^{+4.97} _{-4.18}	0.15 ^{+0.63} _{-0.73}	0.83 ^{+0.12} _{-0.19}	18.72 ^{+0.01} _{-0.01}	0.44 ^{+0.23} _{-0.52}	2682.4
259-G0	–	7879.72 ^{+0.52} _{-0.50}	0.05 ^{+0.01} _{-0.01}	116.10 ^{+10.92} _{-10.07}	–	–	18.95 ^{+0.01} _{-0.01}	0.41 ^{+0.07} _{-0.08}	56.7
259-G+	7879.0	7879.67 ^{+0.62} _{-0.61}	0.08 ^{+0.03} _{-0.03}	87.46 ^{+37.75} _{-18.57}	0.10 ^{+0.12} _{-0.12}	0.14 ^{+0.10} _{-0.10}	18.95 ^{+0.01} _{-0.01}	0.13 ^{+0.30} _{-0.32}	58.8
259-G-	7879.00	7879.99 ^{+0.62} _{-0.58}	-0.08 ^{+0.03} _{-0.03}	85.10 ^{+45.45} _{-20.17}	0.14 ^{+0.12} _{-0.12}	0.09 ^{+0.15} _{-0.13}	18.95 ^{+0.01} _{-0.01}	0.11 ^{+0.35} _{-0.37}	54.1
259-GSA0	–	7880.04 ^{+0.41} _{-0.38}	0.05 ^{+0.01} _{-0.01}	122.34 ^{+9.39} _{-8.47}	–	–	18.99 ^{+0.01} _{-0.01}	0.44 ^{+0.06} _{-0.06}	135.8
259-GSA+	7879.0	7879.92 ^{+0.42} _{-0.39}	0.06 ^{+0.01} _{-0.01}	106.23 ^{+14.73} _{-10.62}	0.01 ^{+0.03} _{-0.03}	0.12 ^{+0.06} _{-0.07}	18.99 ^{+0.00} _{-0.00}	0.31 ^{+0.12} _{-0.12}	258.3
259-GSA-		7880.17 ^{+0.45} _{-0.41}	-0.07 ^{+0.01} _{-0.01}	98.35 ^{+15.25} _{-10.59}	0.16 ^{+0.07} _{-0.07}	0.03 ^{+0.03} _{-0.04}	18.99 ^{+0.01} _{-0.01}	0.25 ^{+0.13} _{-0.13}	124.9
270-G0	–	7511.88 ^{+0.06} _{-0.06}	0.63 ^{+0.01} _{-0.01}	76.71 ^{+0.65} _{-0.39}	–	–	19.09 ^{+0.01} _{-0.01}	0.01 ^{+0.02} _{-0.01}	6729.1
270-G+	7511.0	7513.77 ^{+0.10} _{-0.10}	0.60 ^{+0.01} _{-0.02}	78.58 ^{+1.62} _{-1.19}	-0.01 ^{+0.03} _{-0.02}	-0.16 ^{+0.01} _{-0.01}	19.10 ^{+0.01} _{-0.01}	0.04 ^{+0.05} _{-0.03}	6063.0
270-G-		7513.72 ^{+0.12} _{-0.12}	-0.60 ^{+0.02} _{-0.01}	77.95 ^{+1.75} _{-1.59}	0.02 ^{+0.04} _{-0.05}	-0.16 ^{+0.01} _{-0.01}	19.10 ^{+0.01} _{-0.01}	0.05 ^{+0.05} _{-0.03}	6064.3

Table A.3. continued.

<i>Gaia</i> DR3- ULENS-	$t_{0,\text{par}}$	t_0	u_0	t_E	π_{EN}	π_{EE}	$l_{0,G}$	$f_{b,G}$	χ^2
275-G0	–	7247.41 ^{+0.22} _{–0.22}	0.02 ^{+0.01} _{–0.01}	184.31 ^{+16.93} _{–14.97}	–	–	19.13 ^{+0.01} _{–0.00}	0.73 ^{+0.03} _{–0.03}	163.8
275-G+	7248.0	7247.92 ^{+0.27} _{–0.25}	0.02 ^{+0.02} _{–0.01}	136.61 ^{+27.53} _{–19.58}	0.09 ^{+0.03} _{–0.02}	0.04 ^{+0.09} _{–0.09}	19.11 ^{+0.01} _{–0.01}	0.62 ^{+0.07} _{–0.08}	147.7
275-G-		7247.93 ^{+0.25} _{–0.25}	–0.02 ^{+0.01} _{–0.02}	137.04 ^{+32.74} _{–21.34}	0.04 ^{+0.10} _{–0.11}	0.09 ^{+0.03} _{–0.02}	19.11 ^{+0.01} _{–0.01}	0.63 ^{+0.08} _{–0.09}	138.0
284-G0	–	7841.30 ^{+0.01} _{–0.01}	0.03 ^{+0.01} _{–0.01}	20.67 ^{+0.01} _{–0.01}	–	–	19.31 ^{+0.01} _{–0.01}	0.01 ^{+0.01} _{–0.01}	9662.2
284-G+1		7841.30 ^{+0.01} _{–0.01}	0.03 ^{+0.01} _{–0.01}	20.71 ^{+0.01} _{–0.01}	0.97 ^{+0.02} _{–0.05}	–0.01 ^{+0.02} _{–0.02}	19.31 ^{+0.01} _{–0.01}	0.01 ^{+0.01} _{–0.01}	9631.4
284-G+2	7841.0	7841.30 ^{+0.01} _{–0.01}	0.03 ^{+0.01} _{–0.00}	20.70 ^{+0.01} _{–0.01}	–0.97 ^{+0.05} _{–0.02}	–0.10 ^{+0.02} _{–0.02}	19.31 ^{+0.01} _{–0.01}	0.01 ^{+0.01} _{–0.01}	9624.1
284-G-1		7841.30 ^{+0.01} _{–0.01}	–0.03 ^{+0.01} _{–0.01}	20.76 ^{+0.01} _{–0.01}	0.97 ^{+0.02} _{–0.05}	–0.01 ^{+0.02} _{–0.02}	19.31 ^{+0.01} _{–0.01}	0.01 ^{+0.01} _{–0.01}	9625.3
284-G-2		7841.30 ^{+0.01} _{–0.01}	–0.03 ^{+0.01} _{–0.01}	20.65 ^{+0.01} _{–0.01}	–0.97 ^{+0.05} _{–0.02}	–0.10 ^{+0.02} _{–0.02}	19.31 ^{+0.01} _{–0.01}	0.01 ^{+0.01} _{–0.01}	9629.7
326-G0	–	7048.69 ^{+2.78} _{–2.50}	0.07 ^{+0.08} _{–0.05}	67.15 ^{+2.59} _{–2.44}	–	–	18.03 ^{+0.01} _{–0.01}	0.06 ^{+0.09} _{–0.05}	131.0
326-G+	7316.0	7352.39 ^{+2.41} _{–2.43}	0.37 ^{+0.09} _{–0.06}	157.60 ^{+15.67} _{–16.51}	–0.14 ^{+0.02} _{–0.02}	0.12 ^{+0.01} _{–0.01}	19.94 ^{+0.01} _{–0.01}	0.45 ^{+0.10} _{–0.17}	5563.0
326-G-		7339.19 ^{+1.39} _{–1.48}	–0.59 ^{+0.01} _{–0.01}	111.63 ^{+2.96} _{–2.68}	0.18 ^{+0.02} _{–0.02}	0.14 ^{+0.01} _{–0.01}	19.94 ^{+0.01} _{–0.01}	0.01 ^{+0.02} _{–0.01}	5639.6
331-G0	–	7679.31 ^{+0.03} _{–0.03}	0.10 ^{+0.01} _{–0.01}	74.81 ^{+0.35} _{–0.23}	–	–	20.01 ^{+0.01} _{–0.01}	0.00 ^{+0.01} _{–0.00}	5805.2
331-G+	7694.0	7679.19 ^{+0.15} _{–0.14}	0.09 ^{+0.01} _{–0.01}	75.99 ^{+1.62} _{–0.91}	0.05 ^{+0.08} _{–0.07}	–0.01 ^{+0.02} _{–0.01}	20.01 ^{+0.01} _{–0.01}	0.02 ^{+0.02} _{–0.01}	5806.9
331-G-		7679.30 ^{+0.16} _{–0.14}	–0.10 ^{+0.01} _{–0.01}	75.84 ^{+1.62} _{–0.90}	0.01 ^{+0.08} _{–0.08}	–0.01 ^{+0.01} _{–0.01}	20.01 ^{+0.01} _{–0.01}	0.02 ^{+0.02} _{–0.01}	5805.2
343-G0	–	7890.74 ^{+0.01} _{–0.01}	0.02 ^{+0.01} _{–0.01}	124.88 ^{+0.02} _{–0.02}	–	–	20.31 ^{+0.01} _{–0.01}	0.01 ^{+0.01} _{–0.01}	24865.7
343-G+	7890.0	7890.71 ^{+0.01} _{–0.01}	0.02 ^{+0.01} _{–0.01}	116.70 ^{+0.15} _{–0.14}	0.29 ^{+0.01} _{–0.01}	0.12 ^{+0.01} _{–0.01}	20.24 ^{+0.01} _{–0.01}	0.01 ^{+0.01} _{–0.01}	21902.3
343-G-		7890.71 ^{+0.01} _{–0.01}	0.02 ^{+0.01} _{–0.01}	116.70 ^{+0.15} _{–0.14}	0.29 ^{+0.01} _{–0.01}	0.12 ^{+0.01} _{–0.01}	20.24 ^{+0.01} _{–0.01}	0.01 ^{+0.01} _{–0.01}	21902.3
353-G0	–	7844.70 ^{+0.13} _{–0.13}	0.30 ^{+0.01} _{–0.01}	122.79 ^{+0.88} _{–0.85}	–	–	20.48 ^{+0.01} _{–0.1}	0.01 ^{+0.01} _{–0.01}	7074.2
353-G+	7844.0	7844.80 ^{+0.18} _{–0.19}	0.28 ^{+0.01} _{–0.02}	119.74 ^{+5.54} _{–3.23}	0.23 ^{+0.02} _{–0.02}	–0.02 ^{+0.01} _{–0.01}	20.50 ^{+0.01} _{–0.01}	0.06 ^{+0.08} _{–0.04}	6809.1
353-G-1		7844.60 ^{+0.14} _{–0.15}	–0.30 ^{+0.00} _{–0.00}	105.35 ^{+1.93} _{–1.87}	–0.41 ^{+0.03} _{–0.03}	–0.04 ^{+0.01} _{–0.01}	20.48 ^{+0.01} _{–0.01}	0.01 ^{+0.01} _{–0.01}	6856.7
353-G-2		7846.23 ^{+0.34} _{–0.34}	–0.30 ^{+0.00} _{–0.00}	180.14 ^{+6.65} _{–6.23}	0.32 ^{+0.02} _{–0.02}	–0.07 ^{+0.01} _{–0.01}	20.49 ^{+0.01} _{–0.01}	0.01 ^{+0.01} _{–0.00}	6897.9
359-G0	–	7653.44 ^{+0.03} _{–0.02}	0.09 ^{+0.01} _{–0.01}	93.37 ^{+0.15} _{–0.14}	–	–	20.67 ^{+0.01} _{–0.01}	0.01 ^{+0.01} _{–0.01}	4466.8
359-G+	7653.0	7652.78 ^{+0.03} _{–0.03}	0.02 ^{+0.00} _{–0.00}	367.84 ^{+52.14} _{–46.13}	–0.31 ^{+0.03} _{–0.03}	–0.12 ^{+0.01} _{–0.02}	20.70 ^{+0.01} _{–0.01}	0.80 ^{+0.02} _{–0.03}	2720.4
359-G-		7652.80 ^{+0.03} _{–0.03}	–0.02 ^{+0.01} _{–0.01}	315.82 ^{+36.72} _{–33.09}	0.39 ^{+0.03} _{–0.03}	–0.10 ^{+0.01} _{–0.01}	20.87 ^{+0.01} _{–0.01}	0.72 ^{+0.03} _{–0.03}	2748.0
363-G0	–	7797.53 ^{+0.75} _{–0.78}	0.18 ^{+0.01} _{–0.01}	163.86 ^{+8.09} _{–7.67}	–	–	20.94 ^{+0.01} _{–0.01}	0.40 ^{+0.04} _{–0.04}	5406.7
363-G+	7797.0	7798.92 ^{+0.70} _{–0.73}	0.24 ^{+0.02} _{–0.02}	97.40 ^{+8.11} _{–4.33}	0.25 ^{+0.02} _{–0.02}	0.18 ^{+0.02} _{–0.02}	20.96 ^{+0.02} _{–0.01}	0.08 ^{+0.10} _{–0.06}	5240.3
363-G-1		7800.05 ^{+0.87} _{–0.93}	–0.24 ^{+0.01} _{–0.01}	109.91 ^{+3.81} _{–2.71}	0.27 ^{+0.01} _{–0.01}	0.32 ^{+0.02} _{–0.03}	20.97 ^{+0.01} _{–0.01}	0.03 ^{+0.04} _{–0.02}	5252.3
363-G-2		7798.90 ^{+0.68} _{–0.73}	–0.24 ^{+0.02} _{–0.01}	95.51 ^{+6.40} _{–3.65}	–0.28 ^{+0.02} _{–0.02}	0.19 ^{+0.02} _{–0.02}	20.96 ^{+0.02} _{–0.02}	0.07 ^{+0.09} _{–0.05}	5240.7